Mapping drug-microenvironment-genetic interplay in CLL reveals trisomy 12 as a modulator of microenvironmental signals

Short Title for Running Head:

Drug-microenvironment-genetic interplay in CLL

Peter-Martin Bruch*[1,2], Holly A. R. Giles*[1-4], Carolin Kolb[1,2], Sophie A. Herbst[1-3,5], Tina Becirovic[1], Tobias Roider[1-3], Junyan Lu[3], Sebastian Scheinost[5,7], Lena Wagner[5,7], Jennifer Huellein[3], Ivan Berest[3], Mark Kriegsmann[6], Katharina Kriegsmann[1], Christiane Zgorzelski[6], Peter Dreger[1], Judith B. Zaugg[2,3], Carsten Müller-Tidow[1,2], Thorsten Zenz[8], Wolfgang Huber*[2,3], Sascha Dietrich*[1-3,5]

*These authors contributed equally.

1. Department of Medicine V, University of Heidelberg, Heidelberg, Germany
2. Molecular Medicine Partnership Unit (MMPU), Heidelberg, Germany
3. EMBL Heidelberg, Heidelberg, Germany
4. Collaboration for joint PhD degree between EMBL and Heidelberg University, Faculty of Biosciences, Heidelberg, Germany
5. German Cancer Research Center (DKFZ), Heidelberg, Germany
6. Institute of Pathology, University of Heidelberg, Heidelberg, Germany
7. National Center for Tumour Diseases, Heidelberg, Germany
8. Department of Hematology, University of Zürich, Zürich, Switzerland

Corresponding Author Details

Name: Sascha Dietrich

Address: Im Neuenheimer Feld 410, 69120 Heidelberg, Germany

Email: Sascha.Dietrich@med.uni-heidelberg.de

Phone: 06221/56-39894 06621/56-310977

Fax number: 06221/56-5736

Name: Wolfgang Huber

Address: Meyerhofstraße 1, 69117 Heidelberg, Germany

Email: wolfgang.huber@embl.de

Phone: +49 6221 387-8823

Fax number: +49 6221 387-8166

Presented in abstract form at the 61st annual meeting of the American Society of Hematology, Orlando, FL, 13 November 2019[1]**.**

Key Points:

1) The tumour microenvironment has distinct effects in patient subgroups and modulates drug sensitivity and CLL proliferative capacity.
2) Systematic dataset identifies trisomy 12 and JAK-STAT signalling as important players in cell-extrinsic drug resistance mechanisms.

Abstract

The tumour microenvironment and gene mutations collectively influence drug efficacy in Chronic Lymphocytic Leukaemia (CLL), however an integrative understanding of their interplay is missing. We performed a combinatorial assay using 12 drugs individually co-applied with each of 17 microenvironmental stimuli in 192 primary CLL samples, generating a comprehensive map of drug-microenvironment interactions in CLL. We combined our data with whole-exome sequencing, DNA-methylation, RNA-sequencing and copy number variant data. We complemented these experiments by staining healthy and CLL-infiltrated lymph nodes for downstream mediators of key microenvironmental pathways. Our assay identified four distinct CLL subgroups that differed in their responses to the panel of stimuli and in patient outcomes, distinct from known prognostic groups. Additionally, we identified trisomy 12 as an amplifier of responses to the stimuli, mediated by the transcription factors Spi-B and PU.1. We quantified the impact of the stimuli on drug response, distinguished antagonistic and synergistic combinations and characterised their dependency on genetic alterations. The most frequent modulators of drug responses were stimuli activating Interleukin (IL) 4 and Toll-Like Receptor 7/8/9 signaling. Both pathways were more active in CLL-infiltrated lymph nodes than in healthy samples ($p<0.001$), and high IL4 activity in lymph nodes correlated with shorter survival ($p=0.038$). We provide a publically-available resource to investigate microenvironmental, genetic and drug interplay in CLL. Our results highlight the importance of tumour cell extrinsic influences on drug response and disease progression, and how these are further modulated by cell intrinsic molecular features.

Introduction

CLL is a common B-cell malignancy, attributed to the accumulation of mature B-lymphocytes in the peripheral blood, bone marrow, and lymph nodes[2]. The disease course is heterogeneous, influenced by multiple factors including B cell receptor (BCR) signalling, genetic alterations, epigenetic effects and the tumour microenvironment[3]. Despite significant improvements to CLL treatment, including the advent of BCR inhibitors[4] and BH3-mimetics[5], CLL remains incurable. There is a compelling need to better understand cell-intrinsic and extrinsic causes of therapy failure.

The genetic landscape of CLL is well characterised. The most important features include del(17p), *TP53*-mutations, immunoglobulin heavy chain gene (IGHV) mutation status, del(13q) and trisomy 12[6,7]. This list of recurrent genetic and structural alterations has expanded in the past years[8], and is increasingly being used for treatment stratification.

Additionally to cell-intrinsic factors, CLL cell proliferation and survival is dependent on the lymph node microenvironment[9], which is underlined by the observation that CLL cells undergo spontaneous apoptosis *in vitro* if deprived of these signals[10]. Microenvironmental stimuli can induce drug resistance in vitro, for example, the combination of IL2 and Toll-Like Receptor (TLR) stimulation induces resistance to venetoclax[11]. The CLL microenvironment constitutes a complex network of stromal and immune cells that promote cell expansion[12] via soluble factors and cell-cell contacts. Microenvironmental signaling is particularly important in protective niches, especially lymph nodes. Incomplete response to BCR inhibitors has been linked to persistent enlargement of lymph nodes[13], which are the main site of CLL proliferation[9].

Several studies have investigated individual components of the microenvironment in leukaemia[14–18]. However systematic studies, particularly those exploring cell-extrinsic influences on drug response, are rare. Carey et al.[19] have screened acute myeloid leukemia samples with a panel of soluble factors and among them identified IL1ß as a mediator of

cellular expansion in Acute Myeloid Leukemia. This example highlights the value of systematic approaches to dissect tumour-microenvironment cross-talk.

Taking this approach further, we screened a panel of microenvironmental stimuli in CLL, individually and in combination with drugs, and complemented our dataset with multi-omics data on the patient samples. In this study, we integrate genetic, epigenetic and microenvironmental modulators of drug response in CLL systematically in a large patient cohort that covers the clinical and molecular diversity of CLL. Layer by layer, we develop an integrative understanding of the pathways underlying survival and drug efficacy in CLL.

Methods

Sample preparation and drug-stimulation profiling

Sample preparation, cell-culture, drug-stimulation profiling and genomic annotation was performed on 192 CLL patient samples as previously described[20] with the following adjustments. Stimuli and drugs were mixed and preplated in the culture plates directly before adding the cell suspensions. RPMI-1640 and supplements were acquired from Gibco by Life Technologies, human serum was acquired from PAN Biotech (Cat.No. P40-2701, Lot.No:P-020317). Luminescence was measured after 48h on a Perkin Elmer EnVision.

Compounds and Stimuli

Compounds and stimulatory agents were dissolved, stored and diluted according to manufacturer's protocol. HS-5 conditioned medium was produced by incubating HS-5 stromal cell line to >80% confluency and cell removal by centrifugation. For a detailed list of stimuli and drugs and associated concentrations see Supp. Tables 1 and 2. Final DMSO concentration did not exceed 0.3%.

Spi-B and PU.1 shRNA Knockdown

shRNAs directed against PU.1 (shRNA: 5'-GAAGAAGCTCACCTACCAGTT-3')[21] and Spi-B (shRNA: 5'-CAAGGTTCCCTCTTGTCAGAT-3')[22] were integrated into the pLKO.1 vector backbone (Addgene plasmid #10878) according to the manufacturer's protocol using pLKO.1-scramble shRNA (Addgene plasmid #1864) as control.

Lentiviruses were produced by co-transfecting psPAX2 (4.8 µg; Addgene plasmid #12260), pMD2.G (3.2 µg; Addgene plasmid #12259) and one of the cloned shRNA plasmids (8 µg) to HEK 293T cells. Virus-containing medium was collected 48 and 72 h post transfection and concentrated via ultracentrifugation. The target cells were transduced in 96-well plates and sufficient amounts of virus were added to transduce about 80% of the cells. Spinoculation was performed in the presence of polybrene (SU-DHL 4, SU-DHL 5: 8 µg/mL; SU-DHL 2: 12 µg/mL) for 45 min at 3,200g. At 72h post infection, the cells were selected with puromycin (0.5 µg/mL).

132 For the PU.1/Spi-B Double-KD, the Spi-B-KD cell lines were additionally transduced with the
133 PU.1-KD lentivirus in the same manner as in the first transduction. Knockdown efficiencies
134 were confirmed by PU.1 and Spi-B western blots.

135 **Immunohistochemistry**

136 Lymph node biopsies of CLL-infiltrated and non-neoplastic samples were formalin fixed and
137 paraffin embedded, arranged in Tissue Microarrays and stained for pSTAT6 (ab28829,
138 Abcam) and pIRAK4 (ab216513, Abcam). The slides were analysed using Qupath[23] and the
139 recommended protocol.

140

141 **Data processing and statistical analysis**

142 To quantify the responses to drugs and stimuli, we used a measure of viability relative to the
143 control, namely the natural logarithm of the ratio between CellTiter Glo luminescence readout
144 of the respective treatment and the median of luminescence readouts of the DMSO control
145 wells on the same plate, excluding controls on the outer plate edges. Data analysis was
146 performed using R version 4 and using packages including DESeq2[24], survival[25], Glmnet[26],
147 ConsensusClusterPlus[27], clusterProfiler[28], ChIPseeker[29], genomation[30] and
148 BloodCancerMultiOmics2017[31] to perform univariate association tests, multivariate regression
149 with and without lasso penalization, Cox regression, generalised linear modelling and
150 clustering. The complete analysis is described along with computer-executable transcripts at
151 github.com/Huber-group-EMBL/CLLCytokineScreen2021.

152

153 **ATACseq analysis**

154 For Fig 4B, we selected the raw sequencing files from Rendeiro et al. 2016[32] to include one
155 sample per patient passing quality checks (n=52). We obtained bam files mapped to the hg19
156 genome, adjusted for CG bias, as previously outlined[33]. As trisomy 12 status was not already
157 annotated, we called trisomy 12 in samples that contained > 1.4 times more reads per peak
158 on average in chromosome 12, compared to peaks on other chromosomes. We used diffTf in
159 permutation mode[33] to investigate differential TF activity between trisomy 12 and non-trisomy

160 12 samples using HOCOMOCO v10[34] and with design formula: "~ sample_processing_batch
161 + sex + IGHV status + trisomy 12".
162
163 **Data Sharing Statement**
164 Screening data and patient annotation used in this study are available at github.com/Huber-
165 group-EMBL/CLLCytokineScreen2021. For original sequencing data and raw viability data
166 please contact the corresponding authors. We obtained CLL ATACseq data[32] from the EGA
167 (EGAD00001002110) and ChIPseq data for Spi-B binding[35] from the NCBI GEO database[36]
168 (GSE56857, GSM1370276).
169

170 **Results**

171 ***Ex-vivo* cell viability assay demonstrates functional diversity of cytokine and**
172 **microenvironmental signalling pathways**

173 We measured the effects of 17 cytokines and microenvironmental stimuli on cell viability in
174 192 primary CLL samples and combined each with 12 drugs to investigate the influence on
175 spontaneous and drug-induced apoptosis. (Fig 1A-C, Supp. Tables 1 -3). Viability was
176 assessed by ATP measurement after 48h and normalised to untreated controls[20].

177

178 The patient samples were characterised by DNA sequencing, mapping of copy number
179 variants, genome-wide DNA-methylation profiling, and RNA-Sequencing[20]. The distribution of
180 genetic features in our cohort is comparable to other studies (Supp. Fig 1)[7].

181

182 To assess the heterogeneity of the response patterns, we calculated Pearson correlation
183 coefficients for each pair of drugs and each pair of stimuli. For the drugs, high correlation
184 coefficients (>0.75) were associated with identical target pathways. For example, drugs
185 targeting the BCR pathway (ibrutinib, idelalisib, PRT062607 and selumetinib) were highly
186 correlated, indicating that our data sensitively and specifically reflect interindividual differences
187 in pathway dependencies (Fig. 1D)[20].

188

189 In contrast, microenvironmental stimuli showed lower correlations, even where stimuli targeted
190 similar pathways (Fig. 1E, Supp. Fig. 2). For example, lower correlations were observed
191 between different stimuli of the JAK-STAT and NfκB pathways, indicating a low degree of
192 redundancy between stimuli. High correlations (R>0.75) were only seen with the TLR stimuli
193 Resiquimod (TLR7/8) and CpG ODN (TLR9) as well as IL4 and IL4 + soluble CD40L (sCD40L),
194 which target near identical receptors and downstream targets.

195 Most stimuli increased CLL viability, underlining the supportive nature of the
196 microenvironment. However, IL6, tumor growth factor β (TGFβ) and TLR7/8/9 agonists in
197 IGHV-mutated (IGHV-M) samples decreased viability (Supp. Fig. 3). The strongest responses

198 were seen with IL4 and TLR7/8/9 agonists, highlighting the potency of these pathways in
199 modulating CLL survival. All screening data can be explored manually (github.com/Huber-
200 group-EMBL/CLLCytokineScreen2021) and interactively, via the shiny app (imbi.uni-
201 heidelberg.de/dietrichlab/CLL_Microenvironment/).

202 **Patterns of responses to microenvironmental stimuli reveal two subgroups of IGHV-M**
203 **CLL with differential aggressiveness**

204 To gain a global overview over the pattern of responses to our set of microenvironmental
205 stimuli across patient samples, we clustered[27] and visualised the response profiles (Fig. 2A).

206 This analysis revealed four functionally-defined subgroups with distinct response profiles. Two
207 clusters (termed C1 & C2) were enriched in IGHV-Unmutated (IGHV-U), two (C3 and C4) in
208 IGHV-M CLL. C1 and C2 showed strong responses to IL4 and TLR7/8/9 agonists. C2 was
209 distinguished by stronger responses to the stimuli overall, in particular to NFκB agonists
210 including IL1β and anti-IgM. C3 responded weakly to the majority of stimuli, while C4 was
211 defined by a decreased viability upon TLR7/8/9 stimulation (Supp Fig. 4).

212 Next, we investigated whether these clusters were associated with differential *in vivo* disease
213 progression of the corresponding patients. We used lymphocyte doubling time and time to next
214 treatment to quantify the proliferative capacity of CLL cells. In line with clinical observations[37],
215 the IGHV-U enriched C1 and C2 showed a shorter lymphocyte doubling time than the IGHV-
216 M enriched C3 and C4. More strikingly, C3 showed a significantly shorter lymphocyte doubling
217 time than C4, indicating a higher proliferative capacity (Fig. 2B).
218

219 This observation was reflected in disease progression rates: The predominantly IGHV-M C3
220 showed a progression dynamic similar to the IGHV-U enriched C1 and C2. C4 however
221 showed a longer time to next treatment than C1, C2 and C3 (Cox proportional hazards model,
222 $p= 0.0014$, <0.001, 0.005 respectively, Fig. 2C, Supp. Fig 5A&B). This points towards a subset

223 of mostly IGHV-M patients with more aggressive disease, which is characterized by its
224 differential response to microenvironmental stimuli.
225
226 To characterise genetic differences between clusters, we calculated predictor profiles for
227 cluster assignment, using multinomial regression with the sample mutation profiles (Fig. 2D).
228 IGHV status was the main predictor of all clusters. Trisomy 12 and *SF3B1* mutations were
229 enriched in C2, which showed enhanced responses to many stimuli. C4, which was associated
230 with slow *in vivo* progression, showed depletion of *TP53*, *ATM*, *RAS*/*RAF* mutations and
231 gain(8q).
232
233 The observed difference in progression dynamics *in vivo* was not explained solely by the
234 known prognostic markers IGHV, trisomy 12, and *TP53*. A multivariate Cox proportional
235 hazards model accounting for these features showed an independent prognostic value of the
236 cluster assignment between C3 and C4 (p=0.039, Supp. Table 4).
237
238 To examine why C3 exhibited faster disease progression than C4, we compared baseline
239 pathway activity at the time of sampling, using RNA-Sequencing (Supp. Fig. 6A). Gene set
240 enrichment analysis revealed that key cytokine gene sets were upregulated in C3, including
241 TNFα signaling via NFκB, indicating higher pathway activity *in vivo* (Fig. 2E, Supp. Fig. 6B). In
242 addition, pathways that indicate more aggressive disease relating to proliferation, metabolism
243 and stress response, were upregulated in C3 (Supp. Fig. 6 C-E).
244
245 Taken together, the patterns of responses to our set of stimuli distinguish two subgroups of
246 IGHV-M CLL (C3 and C4) that are characterized by distinct *in vivo* pathway activities and
247 differential disease progression.
248
249

250 **Microenvironmental signals and genetic features collectively determine malignant cell**
251 **survival**
252 Having observed heterogeneous responses to stimulation, we performed univariate analyses
253 of genetic determinants of stimulus response, including IGHV status, somatic gene mutations,
254 and structural variants (Fig. 3A). We identified at least one genetic feature determined stimulus
255 response for 10/17 stimuli and ≥2 features for 6/17 stimuli (Student's t-tests, FDR = 10%),
256 indicating that CLL viability is controlled both by cell-intrinsic mutations and the cells'
257 microenvironment. The most prominent factors were IGHV status and trisomy 12. Responses
258 to microenvironmental stimuli were largely independent of receptor expression (Supp. Fig. 7).
259
260 To address the possible interplay of multiple genetic factors, we applied linear regression with
261 lasso regularisation to derive for each stimulus a multivariate predictor composed of genetic,
262 IGHV and DNA methylation covariates (Fig. 3B). This revealed at least one genetic predictor
263 for five of the 17 stimuli. Trisomy 12 and IGHV status were again the most common features.
264 Stimulus responses stratified by mutations, along with regression model fits can be explored
265 online.
266
267 **Trisomy 12 is a key modulator of responses to stimuli**
268 Our survey of genetic determinants of stimuli response highlighted trisomy 12 as a modulator
269 of responses to IL4, TGFβ, soluble CD40L + IL4 and TLR stimuli.
270
271 TLR response has previously been shown to depend on the IGHV mutation status[17]; we
272 identified trisomy 12 as a second major determinant of response to TLR stimulation. Among
273 the samples without trisomy 12, those with unmutated IGHV displayed increased viability upon
274 TLR stimulation, whereas the response of IGHV-M samples was more heterogeneous, ranging
275 from a strong decrease to a slight increase in viability. In contrast, trisomy 12 samples in both
276 IGHV-U and M cases responded to TLR agonists with increased viability (Student's t-test,
277 $p<0.001$ and $p=0.018$, Fig. 4A).

278

279 To investigate the incompletely understood role of trisomy 12 in CLL we investigated how it
280 might modulate responses to cell-extrinsic signals. We investigated transcription factor (TF)
281 activity in trisomy 12 CLL using two independent ATAC sequencing datasets and used *diffTF*[33]
282 to identify TFs with differential binding site accessibility. The first, produced by ourselves,
283 comprised two WT and two trisomy 12 samples; the second, taken from Rendeiro et al.,
284 included 43 WT and nine trisomy 12 samples. The binding sites of 92 and nine TFs respectively
285 were more accessible ($p<0.05$) in the trisomy 12 samples (Fig. 4B, Supp. Fig. 8), reflecting a
286 specific signaling signature in trisomy 12 CLL. In both datasets, the top hits were the
287 hematopoietic regulators Spi-B and/or PU.1, which share similar binding motifs and exhibit
288 functional redundancy[38]. These TFs are known to be key regulators of healthy B-cell
289 function[39,40], controlling B-cell responses to environmental cues including CD40L, TLR ligands
290 and IL4[41].

291 To investigate Spi-B and PU.1 activity in lymphoma, we hypothesised that these TFs may
292 modulate proliferation by coordinating transcriptional response to microenvironmental signals.
293 To identify Spi-B and PU.1 target genes, we reanalysed a ChIPseq dataset[35], quantifying
294 binding in lymphoma cell lines and tested functional enrichment of immune signalling pathways
295 amongst Spi-B and PU.1 targets. Using selected KEGG and Reactome genesets, we found
296 that TLR, BCR and TGFβ signalling genes were enriched ($p<0.01$) amongst Spi-B and PU.1
297 targets (Fig. 4C).

298 We next investigated the impact of inhibition of Spi-B and PU.1 on proliferation (Fig. 4D). We
299 generated single and double shRNA knockdowns (due to functional redundancy between the
300 TFs) in lymphoma cell lines, both with (SU-DHL4, SU-DHL5) and without trisomy 12 (SU-
301 DHL2) and measured cell proliferation by cell counts every 24 hours. Single knockdown of Spi-
302 B reduced the proliferation rate in SU-DHL5, whilst the PU.1 single knockdown had a smaller
303 impact. Double KD of Spi-B and PU.1 reduced the proliferation in SU-DHL2 and SU-DHL4,
304 and was lethal in SU-DHL5.

305

306 Taken together, we show trisomy 12 is a modulator of response to microenvironmental
307 signals, and link trisomy 12 to higher activity of Spi-B and PU.1, which regulate genes relating
308 to environmental sensing.

309 **Mapping drug-microenvironment interactions reveals drug resistance and sensitivity**
310 **pathways**

311 Guided by the observation of reduced treatment efficacy in protective niches[13], we examined
312 the effects of the stimuli on drug response.

313 We fitted a linear model (Eqn 1) to quantify how each stimulus modulates drug efficacy beyond
314 its individual effects, such as the impact of the stimuli on baseline viability and spontaneous
315 apoptosis. β_{int}, termed the interaction factor, quantifies how the combined treatment effect
316 differs from the sum of the individual treatment effects.

317

318 $$\log V = \beta_d X_d + \beta_s X_s + \beta_{int} X_d X_s + \varepsilon \qquad \text{Eqn 1}$$

319

320 V represents the viability with a given treatment, β_d, β_s and β_{int} are coefficients for the drug,
321 stimulus and combinatorial terms and X_d and X_s are indicator variables (0 or 1) for the presence
322 or absence of a drug/stimulus. ε is the vector of model residuals.

323

324 45 out of 204 combinations had a β_{int} with $p<0.05$. We classified these into four categories,
325 based on the sign of β_{int} and whether the combination effect was antagonistic or synergistic
326 (Fig. 5A-C).

327

328 Positive antagonistic interactions were the most common category, in which stimuli reversed
329 drug action and increased viability. These interactions could lead to treatment resistance *in*
330 *vivo*. They comprised known resistance mechanisms including the inactivation of ibrutinib by

331 IL4 signalling (Fig. 5D)[15], and previously unknown resistance pathways, notably the effect of
332 Interferon-γ (IFNγ) signalling on ibrutinib response (Fig. 5E).
333
334 6/45 interactions were categorised as negative antagonistic, in which drug action reversed the
335 pro-survival effect of microenvironmental stimulation. These interactions point to strategies to
336 overcome treatment resistance. For instance, Pan-JAK inhibition reduced the increase in
337 viability from sCD40L + IL4 stimulation (Fig. 5F).
338
339 We observed a single positive synergistic case, whereby simultaneous treatment with IFNγ
340 and ralimetinib, a p38 MAPK inhibitor, induced a synergistic increase in viability which was not
341 observed with either single treatment (Fig. 5G), pointing towards an inhibitory effect of p38
342 activity on IFNγ signalling.
343
344 16 combinations showed negative synergistic interactions. For example, TLR9 agonist CpG
345 ODN increased the efficacy of BCR inhibition (Fig. 5H). Interestingly, in samples where TLR
346 stimulation increased viability, the addition of BCR inhibitors (ibrutinib and idelalisib)
347 suppressed this effect, indicating that the increase of viability upon TLR stimulation is
348 dependent on BCR activity. The efficacy of luminespib, a HSP90 inhibitor, increased with
349 various stimuli, including soluble anti-IgM (Fig. 5I).
350
351 Altogether, these results highlight the influence of the microenvironment on drug efficacy and
352 underline the value of microenvironmental stimulation in *ex vivo* studies of drug efficacy.
353
354 **Genetic features affect drug-microenvironment interactions**
355 Next, to investigate to what extent genetic driver mutations modulated the interactions between
356 stimuli and drugs, we fit the linear model in Eqn. (1) in a sample - specific manner.
357

358 This resulted in a sample-specific β_{int} interaction coefficient for each drug - stimulus
359 combination. We looked for associations between the size of β_{int} and genetic features using
360 multivariate regression with L1 (lasso) regularisation, with gene mutations and IGHV status as
361 predictors. We generated a predictor profile for each drug - stimulus combination, considering
362 predictors that were selected in >90% of bootstrapped model fits. In total, we found genetic
363 modulators for 60/204 interactions (Fig 6A, Supp Fig. 9). Trisomy 12 and IGHV status
364 modulated the largest number of interactions.
365
366 For example, we found the value of β_{int} for fludarabine and CpG ODN to be modulated by six
367 genetic factors; most strongly by IGHV status, del(11q) and trisomy 12 (Fig. 6B).
368 In IGHV-M non-trisomy 12 samples, fludarabine efficacy increased in the presence of TLR
369 stimulation, whilst in the other subgroups TLR stimulation induced resistance to fludarabine
370 (Fig. 6C).
371
372 Our approach also identified interactions dependent on single treatment effects. IL4 induced
373 complete resistance to ibrutinib regardless of higher ibrutinib efficacy in trisomy 12 and IGHV-
374 U samples. This highlights the breadth of IL4-induced resistance to ibrutinib in CLL across
375 genetic backgrounds (Fig. 6D, Supp. Fig. 10).
376
377 Overall these findings illustrate how the presence of known genetic alterations determines how
378 drugs and external stimuli interact with each other.
379
380 **The key resistance pathways IL4 and TLR show increased activity in CLL-infiltrated**
381 **lymph nodes**
382
383 Microenvironmental signalling within lymph nodes has been implicated in treatment
384 resistance[9,42–44], though a clear understanding of the mechanisms involved remains missing.
385 Since IL4 and TLR signalling were the most prominent modulators of drug response in our

386 study, we assessed their activity within the lymph node niche. We stained paraffin embedded
387 sections of 100 CLL-infiltrated and 100 non-neoplastic lymph nodes for pSTAT6, an essential
388 downstream target of IL4 (Supp. Fig. 11), and pIRAK4, a downstream target of TLR7/8/9.
389
390 The CLL-infiltrated lymph nodes showed higher levels of pSTAT6 (Fig. 7A) and pIRAK4 (Fig.
391 7B). Examples are shown in Fig. 7C-F.
392
393 To investigate the influence of microenvironmental activity in lymph nodes on CLL disease
394 progression, we correlated staining intensity to treatment free survival. High activity of pSTAT-
395 6 correlated with shorter treatment free survival (Fig. 7G), the same trend could be observed
396 with higher pIRAK4 (Fig. 7H).
397

398 **Discussion**

399 Our work maps the effects of microenvironmental stimuli in the presence of drugs and links
400 these to underlying molecular properties across 192 primary CLL samples. We employ all
401 combinations of 17 stimuli with 12 drugs as a reductionist model of microenvironmental
402 signalling. We account for the confounding effects of spontaneous apoptosis *ex vivo* and
403 dissect the effect of individual microenvironmental stimuli on baseline viability and drug toxicity.
404 The results may serve as building blocks for a more holistic understanding of the interactions
405 of tumour genetics, microenvironment and drug response in complex *in vivo* situations.

406 We discover that CLL subgroups can be extracted from microenvironmental response
407 phenotypes and that this classification is linked to distinct molecular profiles and clinical
408 outcomes. IGHV-M samples with weaker responses to microenvironmental stimuli showed
409 faster disease progression, highlighting the important role microenvironmental signalling may
410 play in CLL pathophysiology.

411 The sensitivity afforded by our approach enabled us to identify drug - stimulus interactions,
412 meaning instances where the effect of a drug on the tumour cells is modulated by a
413 microenvironmental stimulus. Our assay recapitulated known drug-resistance phenomena,
414 such as the impact of IL4 stimulation on ibrutinib and idelalisib[15] and identified new ones,
415 including IFNγ-induced resistance to BCR inhibition. Systematic mapping of drug-stimulus
416 interactions, such as generated in this study, can be used to inform biology-based
417 combinatorial treatments across different entities.

418 We demonstrated the breadth of IL4-induced resistance against kinase inhibitors and
419 chemotherapeutics across a range of genetic backgrounds. IL4 induced complete resistance
420 to BCR inhibitors across genetic subgroups, despite greater BCR inhibitor efficacy in IGHV-U
421 CLL. Further, we observed increased IL4 activity within CLL-infiltrated lymph nodes and the
422 association of higher activity with faster disease progression. Our work highlights the
423 significance of IL4 within the lymph node niche, especially since proliferation[9] and resistance
424 to BCR inhibition[13] is linked to lymph nodes and our recent work suggests T follicular helper

425 cells as a source of IL4[45]. Targeting pathways downstream of IL4, via JAK inhibition, has been
426 reported to improve BCR response in non-responding CLL patients[46].

427 Underneath cell-extrinsic factors that control the apoptotic and proliferative activity of tumour
428 cells in response to drugs there lies the network of cell-intrinsic molecular components. We
429 used multivariate modelling to capture the impact of molecular features on responses to stimuli
430 and drugs. For instance, the response to TLR stimulation depended on IGHV status, trisomy
431 12, del11q, del13q and ATM, reflecting the multiple layers of biology involved. Most strikingly,
432 we observed that TLR stimulation increased fludarabine toxicity in the subgroup of IGHV-M
433 non-trisomy 12 patient samples, while it led to fludarabine resistance in all other backgrounds.
434 This finding, combined with our observation that TLR signalling is highly active in CLL-
435 infiltrated lymph nodes might help explain the heterogeneous effects of chemotherapy in CLL,
436 in particular that fludarabine therapy can achieve lasting remission in IGHV-M, but not in IGHV-
437 U patients.
438
439 Beyond TLR, trisomy 12 modulated a broad range of stimulus responses and drug-stimulus
440 interactions, comparable to the impact of IGHV status. Molecularly, we link the observed
441 trisomy 12 phenotype to higher activity of Spi-B and PU.1, essential regulators of
442 environmental sensing in B-cells[41]. Our observation that Spi-B and PU.1 are essential for
443 proliferation in lymphoma cell lines highlights the potential importance of these TFs in survival
444 and proliferation particularly in trisomy 12 CLL.
445
446 We present a data resource for the study of CLL drug response in the context of cell-intrinsic
447 and cell-extrinsic modulators. The data may inform targeted mechanistic investigations[47] and
448 direct efforts for combination therapies. The entire dataset, including the reproducible analysis,
449 can be downloaded from the online repository (github.com/Huber-group-
450 EMBL/CLLCytokineScreen2021), or explored interactively (imbi.uni-
451 heidelberg.de/dietrichlab/CLL_Microenvironment/).
452

Acknowledgments

We thank the Department of Medicine V, University of Heidelberg, Molecular Medicine Partnership Unit (MMPU), EMBL Heidelberg and DKFZ/Heidelberg Center for Personalized Oncology (DKFZ/HIPO) for technical support and funding. HG was supported by a Joachim-Herz Add-on Fellowship for Interdisciplinary Science. PB was supported by a doctoral scholarship of the Franziska-Kolb foundation. S.D. was supported by the Else Kröner Fresenius Foundation, the German Federal Ministry of Education and Research (SYMPATHY) and the German Research Foundation (SFB873). J.L., S.D. and W.H. were supported by the German Federal Ministry of Education and Research (CompLS project MOFA under grant agreement number 031L0171A). T.R. was supported by a physician scientist fellowship of the Medical Faculty of University Heidelberg and the German Federal Ministry of Education and Research (CompLS project SIMONA under grant agreement number 031L0263A). For experimental technical support and expertise, we thank Mareike Knoll, Angela Lenze, Brian Lai, and Vladimir Benes and Nayara Trevisan Doimo de Azevedohe of the EMBL Genomics Core Facility. We thank EMBL's IT Services for providing data management and computing infrastructure, and Simone Bell for organisational support. We thank Mike Smith and Frederik Ziebell for advice on statistics and analysis, Martina Seiffert for the HS-5 stromal cell line, and Michael Boutros, Moritz Gerstung, Nassos Typas and Simon Anders for their comments on the manuscript and their valued advice.

P.M.B is a MD candidate at the University of Heidelberg. This work is submitted in partial fulfillment of the requirement for the MD. H.A.R.G is a PhD candidate for the joint PhD degree between EMBL and Heidelberg University, Faculty of Biosciences. This work is submitted in partial fulfillment of the requirement for the PhD.

Author contributions

S.D. and P.-M.B, designed the experiments. S.D., W.H., H.A.R.G. and P.-M.B, conceptualised the data analysis. W.H. and S.D. supervised the study. W.H., T.Z. and S.D. conceptualised the multi-omics approach to analyse CLL drug response. P.-M.B, performed the drug-stimulus

profiling experiments with support from C.K., S.S. and L.W.. T.Z., C.M.T. and P.D. provided guidance on experimental protocols. H.A.R.G., P.M.B, J.H., J.L., S.D. performed data processing and curation. H.A.R.G. and P.-M.B, analysed and interpreted the data, with support from W.H., S.D., J.L, S.H. and T.R., and produced the figures with input from W.H. and S.D.. H.A.R.G. performed statistical inference and regression modelling, P.-M.B, performed exploratory analysis and integration with clinical data. T.B. and S.H. performed the shRNA knockdown experiments, J.B.Z. and I.B. provided the ATACseq dataset used in Figure 4 and quantified differential transcription factor activity, M.K., K.K. and C.Z. generated the immunohistochemistry data, and P.-M.B, analysed these data. H.A.R.G. designed and wrote the Shiny app and the software documentation. P.-M.B, and H.A.R.G. wrote the manuscript, with input from S.D. and W.H.. All authors reviewed and edited the manuscript.

Conflict of Interest Disclosures

The authors declare that they have no conflict of interests.

References

1. Bruch P-M, Giles H, Kolb C, et al. Systematic investigation of microenvironmental drug resistance mechanisms in chronic Lymphocytic leukemia. *Blood*. 2019;134(Supplement_1):3363–3363.
2. Fabbri G, Dalla-Favera R. The molecular pathogenesis of chronic lymphocytic leukaemia. *Nat. Rev. Cancer*. 2016;16(3):145–162.
3. Puente XS, Jares P, Campo E. Chronic lymphocytic leukemia and mantle cell lymphoma: crossroads of genetic and microenvironment interactions. *Blood*. 2018;131(21):2283–2296.
4. Burger JA, Tedeschi A, Barr PM, et al. Ibrutinib as Initial Therapy for Patients with Chronic Lymphocytic Leukemia. *N. Engl. J. Med.* 2015;373(25):2425–2437.
5. Fischer K, Al-Sawaf O, Bahlo J, et al. Venetoclax and Obinutuzumab in Patients with CLL and Coexisting Conditions. *N. Engl. J. Med.* 2019;380(23):2225–2236.

509 6. Gaidano G, Rossi D. The mutational landscape of chronic lymphocytic leukemia and its
510 impact on prognosis and treatment. *Hematology Am. Soc. Hematol. Educ. Program*.
511 2017;2017(1):329–337.
512 7. Döhner H, Stilgenbauer S, Benner A, et al. Genomic aberrations and survival in chronic
513 lymphocytic leukemia. *N. Engl. J. Med.* 2000;343(26):1910–1916.
514 8. Strefford JC. The genomic landscape of chronic lymphocytic leukaemia: biological and
515 clinical implications. *Br. J. Haematol.* 2015;169(1):14–31.
516 9. Herndon TM, Chen S-S, Saba NS, et al. Direct in vivo evidence for increased
517 proliferation of CLL cells in lymph nodes compared to bone marrow and peripheral
518 blood. *Leukemia*. 2017;31(6):1340–1347.
519 10. Collins RJ, Verschuer LA, Harmon BV, et al. Spontaneous programmed death
520 (apoptosis) of B-chronic lymphocytic leukaemia cells following their culture in vitro. *Br. J.*
521 *Haematol.* 1989;71(3):343–350.
522 11. Oppermann S, Ylanko J, Shi Y, et al. High-content screening identifies kinase inhibitors
523 that overcome venetoclax resistance in activated CLL cells. *Blood*. 2016;128(7):934–
524 947.
525 12. Ten Hacken E, Burger JA. Microenvironment interactions and B-cell receptor signaling
526 in Chronic Lymphocytic Leukemia: Implications for disease pathogenesis and treatment.
527 *Biochim. Biophys. Acta*. 2016;1863(3):401–413.
528 13. Ahn IE, Farooqui MZH, Tian X, et al. Depth and durability of response to ibrutinib in CLL:
529 5-year follow-up of a phase 2 study. *Blood*. 2018;131(21):2357–2366.
530 14. Chen Z, ter Burg H, Andrejeva G, et al. LINKING MICROENVIRONMENTAL SIGNALS
531 TO METABOLIC SWITCHES AND IBRUTINIB RESPONSE IN CHRONIC
532 LYMPHOCYTIC LEUKEMIA: PS1125. *HemaSphere*. 2019;3:509–510.
533 15. Aguilar-Hernandez MM, Blunt MD, Dobson R, et al. IL-4 enhances expression and
534 function of surface IgM in CLL cells. *Blood*. 2016;127(24):3015–3025.
535 16. Jayappa KD, Portell CA, Gordon VL, et al. Microenvironmental agonists generate
536 phenotypic resistance to combined ibrutinib plus venetoclax in CLL and MCL. *Blood*

537 *Adv*. 2017;1(14):933–946.
538 17. Chatzouli M, Ntoufa S, Papakonstantinou N, et al. Heterogeneous functional effects of
539 concomitant B cell receptor and TLR stimulation in chronic lymphocytic leukemia with
540 mutated versus unmutated Ig genes. *J. Immunol.* 2014;192(10):4518–4524.
541 18. Dietrich S, Krämer OH, Hahn E, et al. Leflunomide induces apoptosis in fludarabine-
542 resistant and clinically refractory CLL cells. *Clin. Cancer Res.* 2012;18(2):417–431.
543 19. Carey A, Edwards DK, Eide CA,et al. Identification of Interleukin-1 by Functional
544 Screening as a Key Mediator of Cellular Expansion and Disease Progression in Acute
545 Myeloid Leukemia. *Cell Rep.* 2017;18(13):3204–3218.
546 20. Dietrich S, Oleś M, Lu J, et al. Drug-perturbation-based stratification of blood cancer. *J.*
547 *Clin. Invest.* 2018;128(1):427–445.
548 21. Libregts SF, Gutiérrez L, de Bruin AM, et al. Chronic IFN-γ production in mice induces
549 anemia by reducing erythrocyte life span and inhibiting erythropoiesis through an IRF-
550 1/PU.1 axis. *Blood*. 2011;118(9):2578–2588.
551 22. Lenz G, Wright GW, Emre NCT, et al. Molecular subtypes of diffuse large B-cell
552 lymphoma arise by distinct genetic pathways. *Proc. Natl. Acad. Sci. U. S. A.*
553 2008;105(36):13520–13525.
554 23. Bankhead P, Loughrey MB, Fernández JA, et al. QuPath: Open source software for
555 digital pathology image analysis. *Sci. Rep.* 2017;7(1):1–7.
556 24. Love MI, Huber W, Anders S. Moderated estimation of fold change and dispersion for
557 RNA-seq data with DESeq2. *Genome Biol.* 2014;15(12):550.
558 25. Therneau TM, Grambsch PM. Modeling Survival Data: Extending the Cox Model.
559 Springer Science & Business Media; 2000.
560 26. Friedman J, Hastie T, Tibshirani R. Regularization Paths for Generalized Linear Models
561 via Coordinate Descent. *J. Stat. Softw.* 2010;33(1):1–22.
562 27. Wilkerson MD, Hayes DN. ConsensusClusterPlus: a class discovery tool with
563 confidence assessments and item tracking. *Bioinformatics*. 2010;26(12):1572–1573.
564 28. Yu G, Wang L-G, Han Y, He Q-Y. clusterProfiler: an R Package for Comparing

565 Biological Themes Among Gene Clusters. *OMICS: A Journal of Integrative Biology*.
566 2012;16(5):284–287.
567 29. Yu G, Wang L-G, He Q-Y. ChIPseeker: an R/Bioconductor package for ChIP peak
568 annotation, comparison and visualization. *Bioinformatics*. 2015;31(14):2382–2383.
569 30. Akalin A, Franke V, Vlahoviček K, Mason CE, Schübeler D. Genomation: a toolkit to
570 summarize, annotate and visualize genomic intervals. *Bioinformatics*. 2015;31(7):1127–
571 1129.
572 31. Malgorzata Oles, Sascha Dietrich, Junyan Lu, Britta Velten, Andreas Mock, Vladislav
573 Kim, Wolfgang Huber. BloodCancerMultiOmics2017. Bioconductor; 2018.
574 32. Rendeiro AF, Schmidl C, Strefford JC, et al. Chromatin accessibility maps of chronic
575 lymphocytic leukaemia identify subtype-specific epigenome signatures and transcription
576 regulatory networks. *Nat. Commun.* 2016;7:11938.
577 33. Berest I, Arnold C, Reyes-Palomares A, et al. Quantification of Differential Transcription
578 Factor Activity and Multiomics-Based Classification into Activators and Repressors:
579 diffTF. *Cell Rep.* 2019;29(10):3147–3159.e12.
580 34. Kulakovskiy IV, Vorontsov IE, Yevshin IS, et al. HOCOMOCO: expansion and
581 enhancement of the collection of transcription factor binding sites models. *Nucleic Acids*
582 *Res.* 2016;44(D1):D116–25.
583 35. Care MA, Cocco M, Laye JP, et al. SPIB and BATF provide alternate determinants of
584 IRF4 occupancy in diffuse large B-cell lymphoma linked to disease heterogeneity.
585 *Nucleic Acids Res.* 2014;42(12):7591–7610.
586 36. Edgar R, Domrachev M, Lash AE. Gene Expression Omnibus: NCBI gene expression
587 and hybridization array data repository. *Nucleic Acids Res.* 2002;30(1):207–210.
588 37. Baumann T, Moia R, Gaidano G, et al. Lymphocyte doubling time in chronic lymphocytic
589 leukemia modern era: a real-life study in 848 unselected patients. *Leukemia*. 2021;
590 38. Garrett-Sinha LA, Dahl R, Rao S, Barton KP, Simon MC. PU.1 exhibits partial functional
591 redundancy with Spi-B, but not with Ets-1 or Elf-1. *Blood*. 2001;97(9):2908–2912.
592 39. Turkistany SA, DeKoter RP. The Transcription Factor PU.1 is a Critical Regulator of

593 Cellular Communication in the Immune System. *Arch. Immunol. Ther. Exp.* .
594 2011;59(6):431–440.
595 40. Ray-Gallet D, Mao C, Tavitian A, Moreau-Gachelin F. DNA binding specificities of Spi-
596 1/PU.1 and Spi-B transcription factors and identification of a Spi-1/Spi-B binding site in
597 the c-fes/c-fps promoter. *Oncogene*. 1995;11(2):303–313.
598 41. Willis SN, Tellier J, Liao Y, et al. Environmental sensing by mature B cells is controlled
599 by the transcription factors PU.1 and SpiB. *Nat. Commun.* 2017;8(1):1426.
600 42. Hayden RE, Pratt G, Roberts C, Drayson MT, Bunce CM. Treatment of chronic
601 lymphocytic leukemia requires targeting of the protective lymph node environment with
602 novel therapeutic approaches. *Leuk. Lymphoma*. 2012;53(4):537–549.
603 43. Mittal AK, Chaturvedi NK, Rai KJ, et al. Chronic lymphocytic leukemia cells in a lymph
604 node microenvironment depict molecular signature associated with an aggressive
605 disease. *Mol. Med.* 2014;20:290–301.
606 44. Yan X-J, Dozmorov I, Li W, et al. Identification of outcome-correlated cytokine clusters in
607 chronic lymphocytic leukemia. *Blood*. 2011;118(19):5201–5210.
608 45. Roider T, Seufert J, Uvarovskii A, et al. Dissecting intratumour heterogeneity of nodal B-
609 cell lymphomas at the transcriptional, genetic and drug-response levels. *Nature Cell*
610 *Biology*. 2020;22(7):896–906.
611 46. Spaner DE, McCaw L, Wang G, Tsui H, Shi Y. Persistent janus kinase-signaling in
612 chronic lymphocytic leukemia patients on ibrutinib: Results of a phase I trial. *Cancer*
613 *Med.* 2019;8(4):1540–1550.
614 47. Lu J, Cannizzaro E, Meier-Abt F, et al. Multi-omics reveals clinically relevant proliferative
615 drive associated with mTOR-MYC-OXPHOS activity in chronic lymphocytic leukemia.
616 *Nat Cancer*. 2021;

617

618

619 **Figure Legends**

620

621 **Figure 1. Study outline and overview of drugs and stimuli.**

622 (A) Schematic of experimental protocol. By combining 12 drugs and 17 stimuli, we
623 systematically queried the effects of simultaneous stimulation and inhibition of critical
624 pathways in CLL (n=192). Integrating functional drug-stimulus response profiling with four
625 additional omics layers, we identified pro-survival pathways, underlying molecular modulators
626 of drug and microenvironment reponses, and drug-stimulus interactions in CLL. All screening
627 data can be explored either manually (github.com/Huber-group-
628 EMBL/CLLCytokineScreen2021 or interactively, via the shiny app (www.imbi.uni-
629 heidelberg.de/dietrichlab/CLL_Microenvironment/). (B) Overview of stimuli included in the
630 screen and summary of their associated targets. HS-5 Culture Medium is omitted, as no
631 specific target can be shown. (C) Table of drugs included in the screen. Drug target, and
632 category of target are also shown. (D and E) Forest plots of Pearson coefficients calculated
633 from selected pairwise drug-drug (D) and stimulus-stimulus (E) correlations. Closely related
634 stimuli targeting the NfKB and JAK-STAT pathways are shown as examples of stimuli which
635 share very similar receptors and downstream target profiles but show a divergence of effects.

636

637 **Figure 2. Ex vivo cell viability assay of CLL primary samples reveals subgroups with**
638 **distinct stimulus response profiles, and differential disease progression.**

639 (A) The heatmap matrix shows the viability measurements for 192 samples (columns) and 17
640 stimuli (rows). Viability was measured via ATP-based assay after 48h stimulation. The data
641 are shown normalised to DMSO-treated controls, and scaled within each row according to the
642 Median Absolute Deviation. Limits were applied to scaling factor for optimal visualisation. The
643 colour bars to the right show sample annotations. Consensus Clustering was used to define
644 column tree layout, using hierarchical clustering with the Euclidean metric. (B) Lymphocyte
645 doubling time, a clinical marker for disease progression, plotted for each cluster. (C) Kaplan-

646 Meier curves of time to next treatment for each cluster. p-values from univariate Cox
647 proportional hazard models comparing IGHV-U enriched C1 with C2, and IGHV-M enriched
648 C3 with C4. (D) Multinomial regression with lasso penalisation to identify enrichment or
649 depletion of genetic features within each cluster. Matrix of genetic features (p=39), and IGHV
650 status (encoded as M = 1 and U = 0) were used to identify multivariate predictors of cluster
651 assignment. x axis shows genetic predictors, y axis indicates value and sign of coefficient
652 assigned to feature, for each cluster (positive coefficients are enriched in the cluster, negative
653 coefficients are depleted). Coefficients shown are mean coefficients from 50 bootstrapped
654 repeats and error bars represent the mean ± standard deviation. Genetic features with >20%
655 missing values were excluded, and only patients with complete annotation were included in
656 the model (n=137). (E) Gene set enrichment analysis (GSEA) to compare expression of genes
657 in samples from C3 and C4 reveals upregulation of Hallmark pathways involved in
658 microenvironmental signalling, stress response, metabolism and proliferation in C3.
659 Normalised enrichment scores are shown for top 10 most significant pathways upregulated in
660 C3 versus C4. Bars coloured according to adjusted p-value. Genes are ranked based on Wald
661 statistic, calculated using the Deseq2 package and GSEA performed using the fgsea
662 algorithm.
663
664 **Figure 3. Responses to microenvironmental signals are modulated by genetic**
665 **alterations recurrent in CLL.**
666 (A) Overview of results of all tested gene - stimulus associations. x-axis shows stimuli, y-axis
667 shows p-values from Student's t-test (two-sided, with equal variance). Tests were performed
668 for somatic mutations and copy number aberrations present in ≥3 patients, and IGHV status
669 (n = 63). Each circle represents a gene-stimulus association. Tests with p-values smaller than
670 the threshold corresponding to a false discovery rate (FDR) of 10% (method of Benjamini and
671 Hochberg) are indicated by colored circles, where the colors represent the gene mutations and
672 structural aberrations. (B) Predictor profiles for selected stimuli to represent gene - stimulus
673 associations identified through Gaussian linear modelling with L1-penalty. Matrix of genetic

674 features (p=39), IGHV status (encoded as M = 1 and U = 0), and Methylation Cluster (encoded
675 as 0, 0.5, 1) were used to identify multivariate predictors. Bar plots on left indicate size and
676 sign of coefficients assigned to the named predictors. Positive coefficients indicate higher
677 viability after stimulation if the feature is present. Scatter plot and heatmap indicate how each
678 genetic feature relates to sample viabilities: Scatter plots indicate log(viability) values, in order
679 of magnitude, for each individual sample. Heatmaps show mutation status for each of the
680 genetic predictors for corresponding sample in scatter plot. Coefficients for sCD40L + IL4 and
681 CpG ODN were also significant, these plots have been omitted to avoid redundancy.
682
683 **Figure 4. Trisomy 12 modulates responses to microenvironmental signals.**
684 (A) Trisomy 12 IGHV-M samples show a strongly positive reaction to TLR stimulation,
685 comparable to IGHV-U samples. Plot shows log transformed viability values, normalised to
686 DMSO controls, after stimulation with the TLR 7/8 agonist Resiquimod. p-values from
687 Student's t-test. (B) Spi-B and PU.1 TF binding sites show higher accessibility in trisomy 12
688 CLL. Bar plot shows change in TF activity (y axis) between between trisomy 12 (n = 9) and
689 non-trisomy 12 samples (n = 43), for all significant TFs (x axis, adjusted p-value <0.05). Data
690 taken from Rendeiro et al 2016[32], and change in TF activity calculated using the diffTF
691 package, and measured as weighted mean difference. p-values are obtained through diffTF
692 in permutation mode and adjusted by the Benjamini-Hochberg procedure. TF binding sites and
693 names from HOCOMOCO database. (C) ChIPseq analysis of Spi-B and PU.1 binding
694 indicates involvement in coordinating transcriptional response to microenvironmental signals,
695 including TLR. Table shows results from over-representation tests of selected KEGG and
696 Reactome pathways amongst Spi-B and PU.1 targets. Columns show geneset pathways,
697 corresponding database, the number of genes within geneset, the number of Spi-B and PU.1
698 target genes within geneset (total number of target genes defined also shown), and p-value
699 from over-representation test. TF targets defined as closest gene to each significant ChIP peak
700 (q value<0.05), and within ±1kb of TSS. ChIPseq data from Care et al. 2014[28]. Over-
701 representation tests run using clusterProfiler package, method corresponds to one-sided

702 version of Fisher's exact test. (D) Knockdown of Spi-B and PU.1 led to growth restriction and
703 cell death. Data shown is the mean of three technical replicates. While SU-DHL 5 was already
704 growth impaired after Spi-B KD, SU-DHL 2 and SU-DHL 4 were only impaired after double
705 knock-down. Double knockdown lead to rapid cell death in SU-DHL 5 (data not shown). Cell
706 count normalised to seeded cell number of diffuse large b cell lymphoma cell lines after
707 knockdown of Spi-B or double knockdown of Spi-B and PU.1 or shRNA as control.
708
709 **Figure 5. Signals from the microenvironment influence ex-vivo drug response.**
710 (A) Graphical representation of the four drug - stimulus interaction categories. Categories are
711 defined according to the nature of the interaction (synergistic or antagonistic), and whether the
712 viability is increased or decreased by the stimulus (positive or negative). x-axis shows
713 treatment type, y-axis shows viability with each treatment. Points (red) depict a representative
714 treatment response pattern for given interaction type. To demonstrate the effect of each
715 interaction on expected viability, blue and black horizontal lines represent the expected
716 viability for combinatorial treatment in the absence of an interaction between drug - stimulus
717 (blue) and the viability for combinatorial treatment with given interaction (black). (B) Histogram
718 to show the number of drug- stimulus interactions within each category, where p value for β_{int}
719 is <0.05. (C) Heatmap of all β_{int} values for all drug - stimulus combinations where p for β_{int}
720 <0.05, annotated with interaction type. Scale indicates size and sign of β_{int}. Rows and columns
721 clustered according to hierarchical clustering. (D - I) Examples of drug-stimulus interactions,
722 for each category. Plots show log transformed viability values with each treatment, for all
723 samples. Matching samples are linked across treatments. Black and blue horizontal lines
724 indicate the predicted viability from the linear model for each single and combinatorial
725 treatment. In combinatorial treatment, both the expected viability based on the additive effect
726 of drug and stimulus (blue), and the viability with interaction (black) are shown, to indicate the
727 impact of the interaction. (D+E) Ibrutinib, a clinically-used BTK inhibitor, is blocked by IL4 and
728 IFNγ. (F) The JAK inhibitor pyridone-6 inhibits the pro-survival effect of sCD40L + IL4
729 stimulation. (G) The p38 inhibitor ralimetinib and IFNγ show a synergistic pro-survival effect

730 not seen in either single treatment. (H) TLR agonists, including CpG ODN (shown) increase
731 sensitivity to BTK inhibition by ibrutinib, despite increasing viability in isolation. (I) Soluble anti-
732 IgM sensitises CLL samples to HSP90 inhibition by luminespib.
733
734 **Figure 6. Integrating the effects of genetic features and stimuli on drug response.**
735 (A) Representative predictor profile depicting genetic features that modulate the size of β_{int}
736 between fludarabine and CpG ODN, to illustrate the approach used. To generate predictor
737 profile, linear model in Eqn. (1) was fitted in a sample - specific manner, to calculate drug-
738 stimulus interaction coefficients (β_{int}) for each patient sample. Ranked patient-specific β_{int}
739 values are shown in lower scatter plot. Associations between the size of β_{int} and genetic
740 features were identified using multivariate regression with L1 (lasso) regularisation, with gene
741 mutations (p = 39) and IGHV status as predictors, and selecting coefficients that were chosen
742 in >90% of bootstrapped model fits. The horizontal bars on left show the size of fitted
743 coefficients assigned to genetic features. Matrix above scatter plot indicates patient mutation
744 status for the selected genetic features. Matrix fields correspond to points in scatter plot (ie
745 patient data is aligned), to indicate how the size of β_{int} varies with selected genetic feature.
746 Grey lines indicate presence of genetic feature/IGHV mutated. (B) Heatmap depicting
747 overview of genetic predictors of drug - stimulus interactions (each row represents the
748 coefficients from fitting a single multivariate model, as in (A)). Stimuli are shown on left, and
749 corresponding drugs on right. Coloured fields indicate that β_{int} for given drug and stimulus is
750 modulated by corresponding genetic feature. Positive coefficients are shown in red, indicating
751 a more positive β_{int} if the feature is present. Only top 8 most commonly selected genetic
752 features are shown. Drug - stimulus combinations with no genetic predictors of β_{int} amongst
753 top 8 shown are omitted for clarity. (C-D) Beeswarm boxplots of log(viability) values, for (C)
754 fludarabine and CpG ODN and (D) ibrutinib and IL4 single and combinatorial treatments,
755 faceted by IGHV status and trisomy 12 status. P-values from paired Student's t-tests.
756
757 **Figure 7. IL4 and TLR signaling are upregulated in CLL-infiltrated lymph nodes.**

758 Lymph node biopsies of CLL-infiltrated and non-neoplastic samples were stained for pSTAT6,
759 a downstream target of IL4, and pIRAK4, a downstream target of TLR, revealing increased
760 signaling activity in CLL-infiltrated lymph nodes. (A-B) Mean pSTAT6 and pIRAK4 staining
761 intensity after background substraction (y axis), p values from Student's t-test. (C-F) Example
762 images of IHC sections. (C, D) shows pSTAT6 levels in (C) CLL-infiltrated and (D) non-
763 neoplastic samples. (E,F) shows pIRAK4 levels in (E) CLL-infiltrated and (F) non-neoplastic
764 samples. (G-H) Kaplan-Meier plots for treatment free survival stratified by levels (high / low)
765 of pSTAT6 (G) and pIRAK4 (H). The two pSTAT6 and pIRAK4 groups were defined by mean
766 staining intensities dichotomised using maximally selected rank statistics. The same 64 CLL
767 lymph node samples were used for both Kaplan-Meier plots. 50 patient samples were in the
768 high pSTAT6 group, and 52 in the high pIRAK4 group.

Figure 1

A

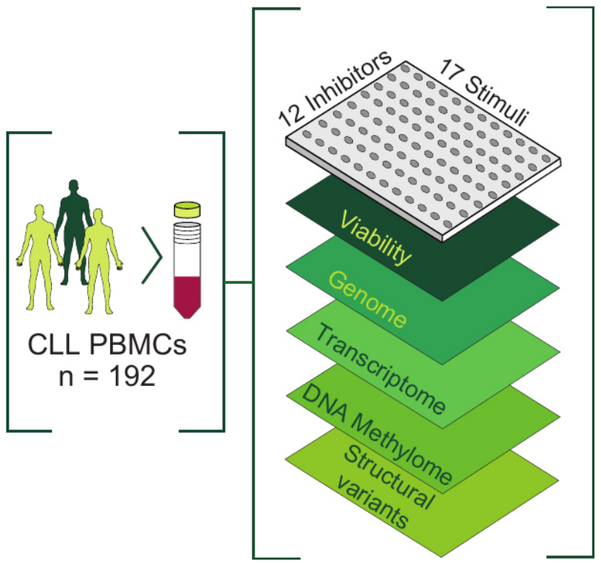

B

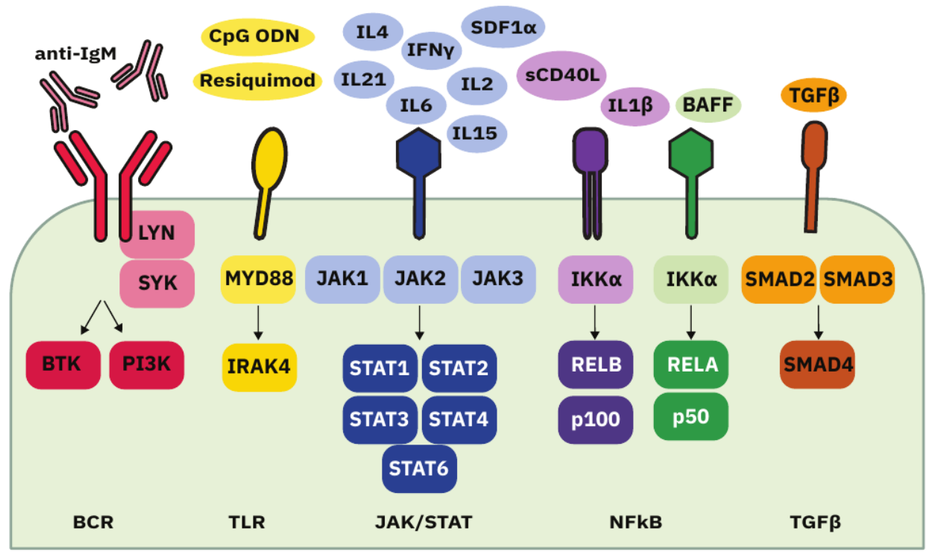

C

Drug	Target	Category
Ibrutinib	BTK	BCR
Idelalisib	PI3K delta	BCR
PRT062607	SYK	BCR
Fludarabine	Purine analogue	DDR
Nutlin-3a	MDM2	DDR
I-BET 762	BRD2/3/4	Epigenome
Luminespib	HSP90	HSP90
Pyridone-6	JAK1/2/3	JAK/STAT
Selumetinib	MEK1/2	MAPK
Ralimetinib	p38 MAPK	MAPK
Everolimus	mTOR	mTOR
BAY-11-7085	NFkB	NFkB

D

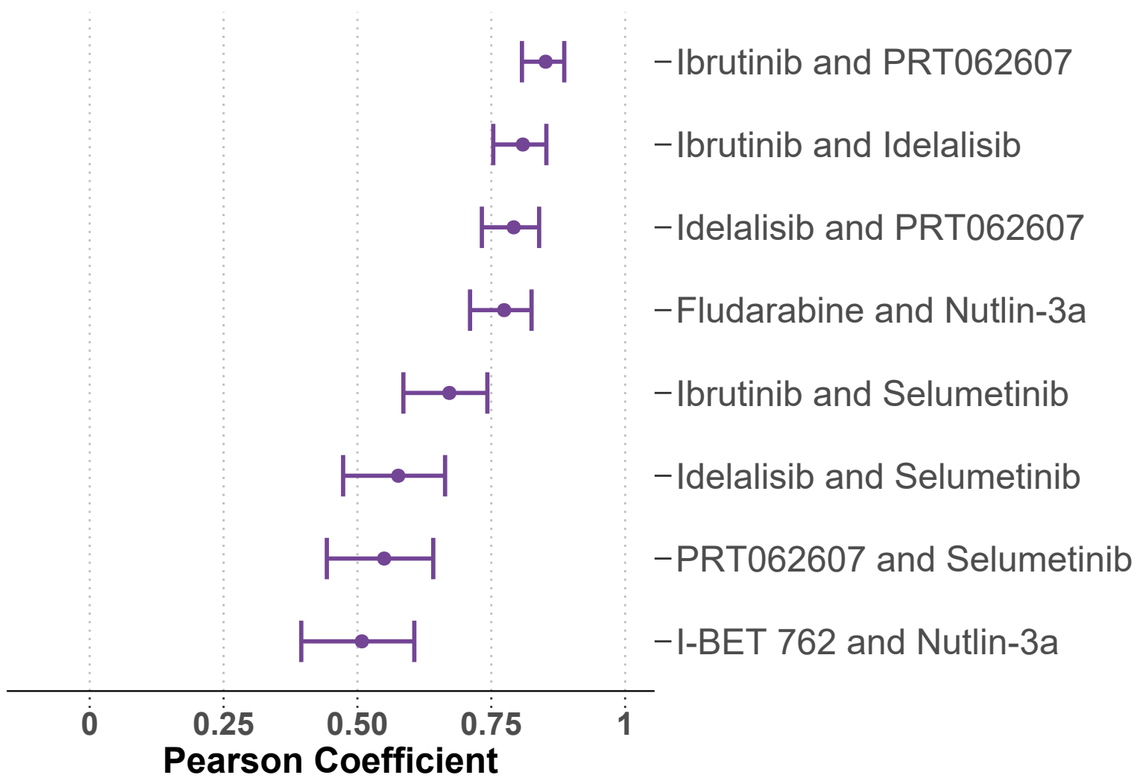

E

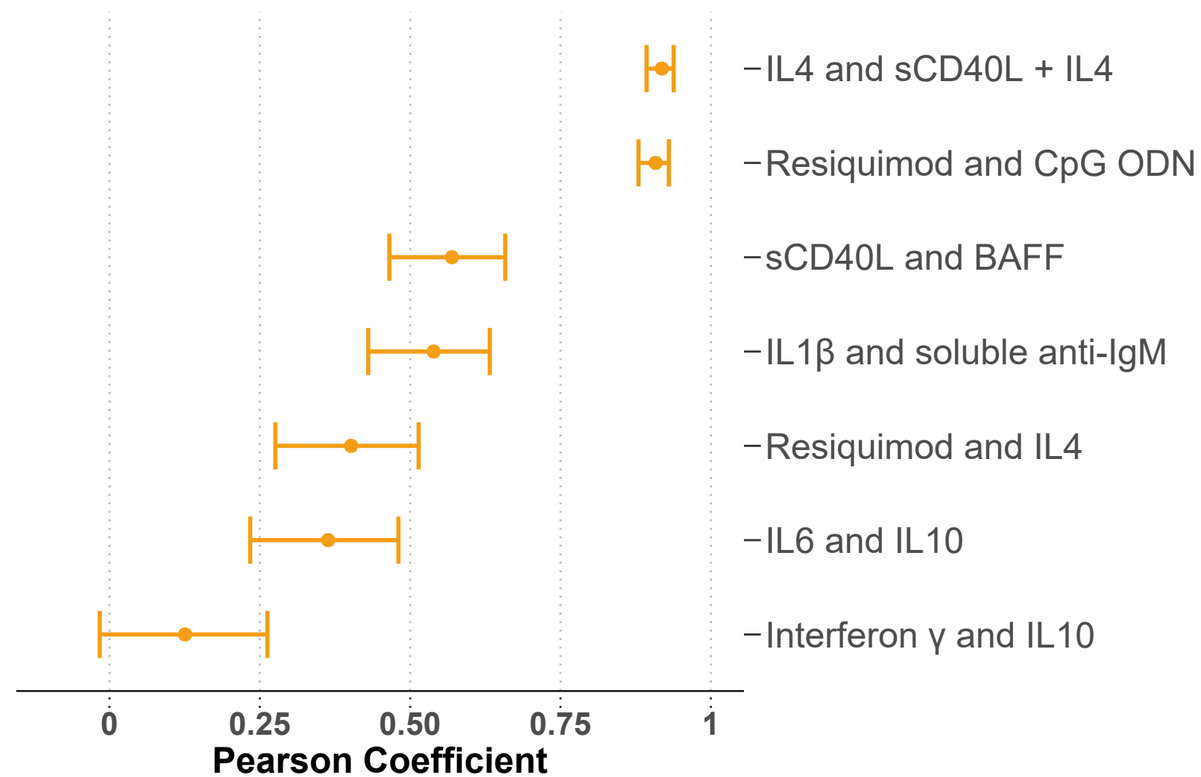

Figure 2

A

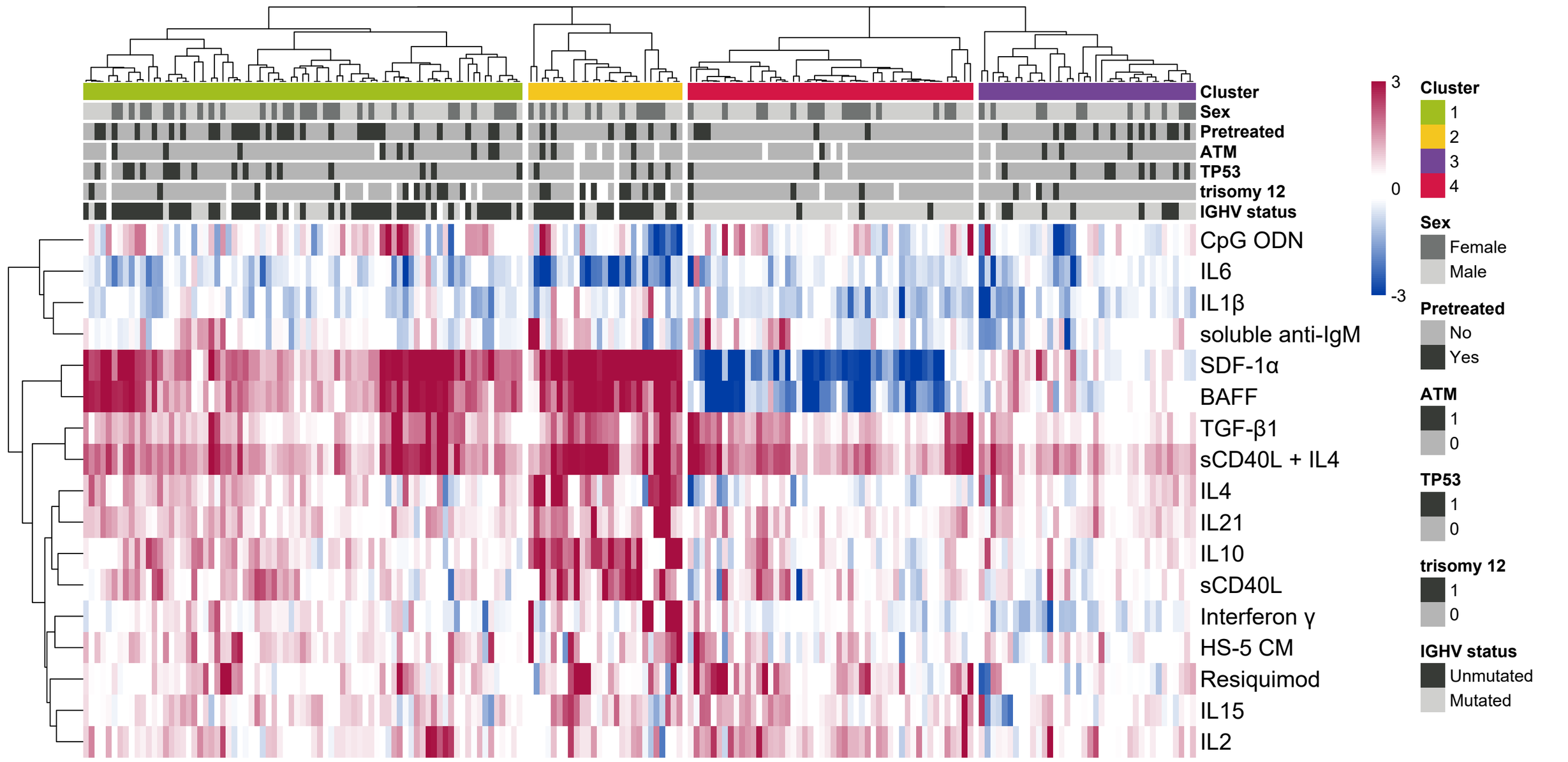

B

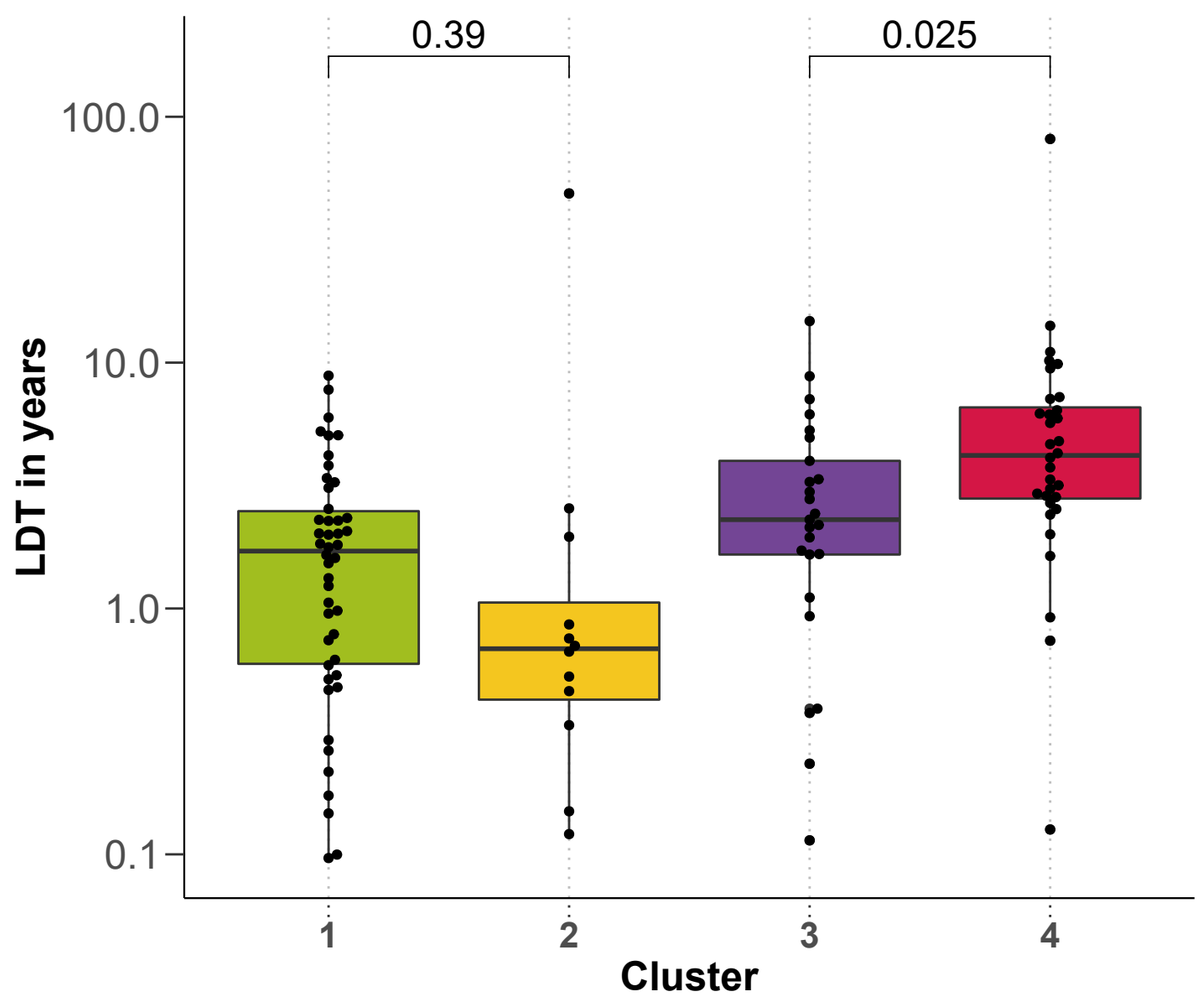

C

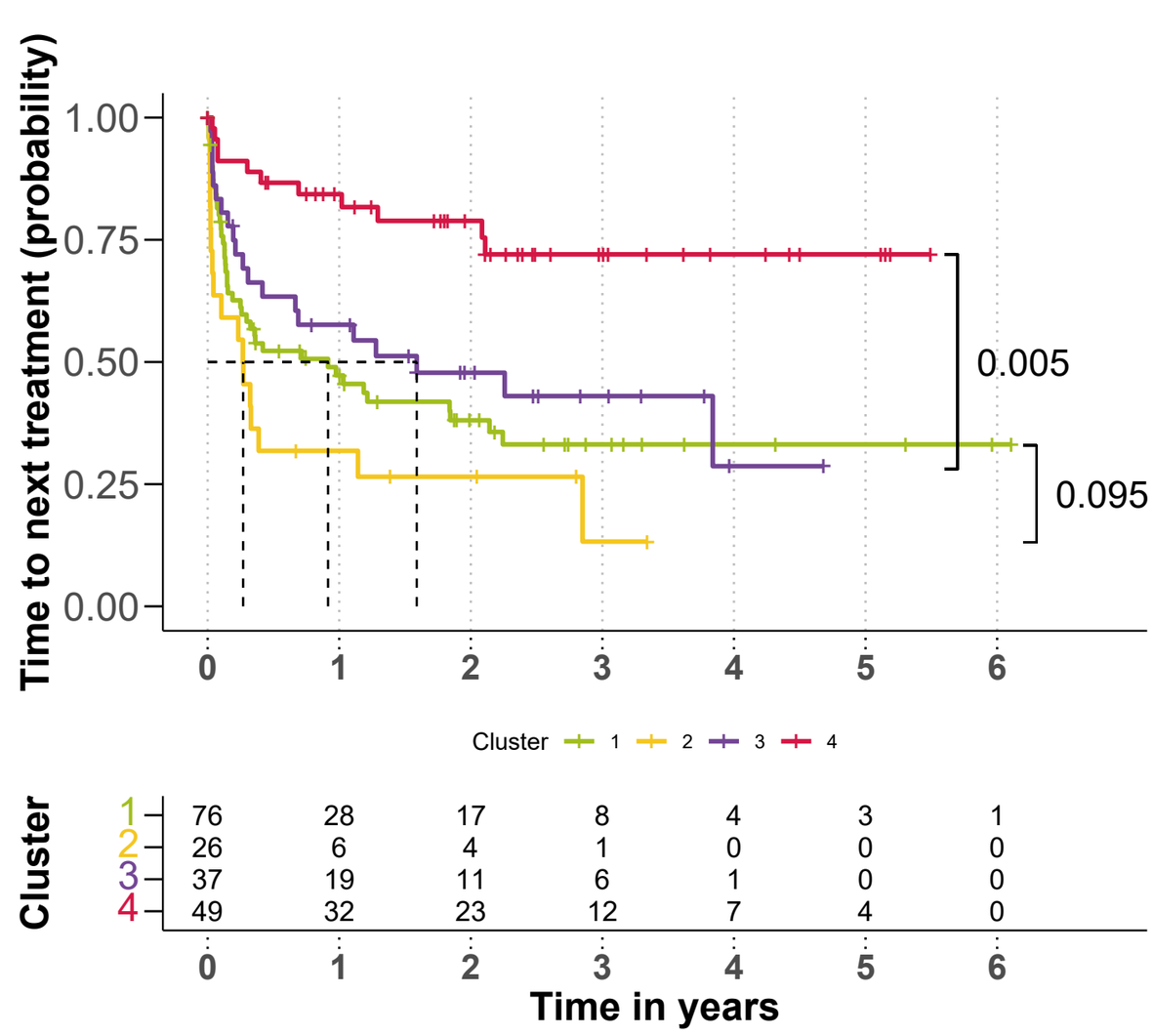

D

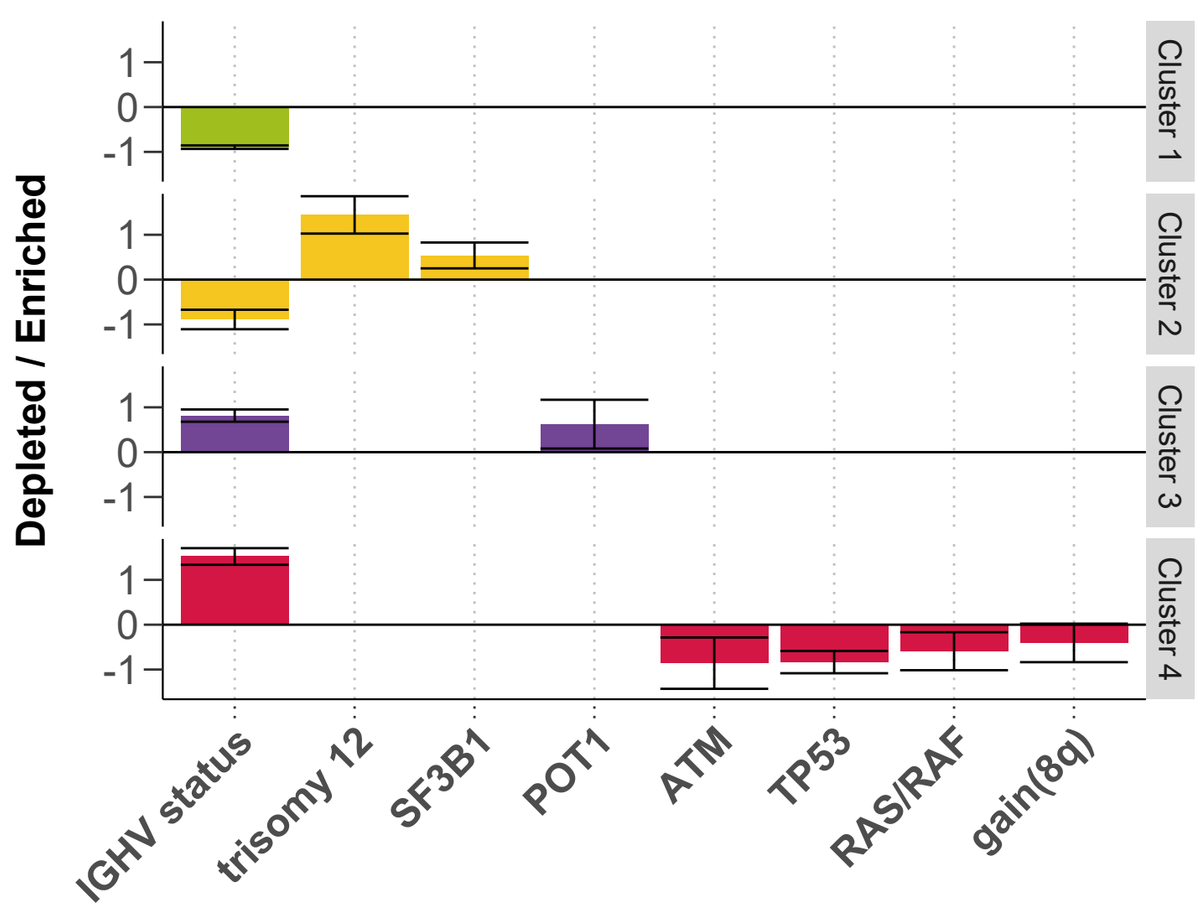

E

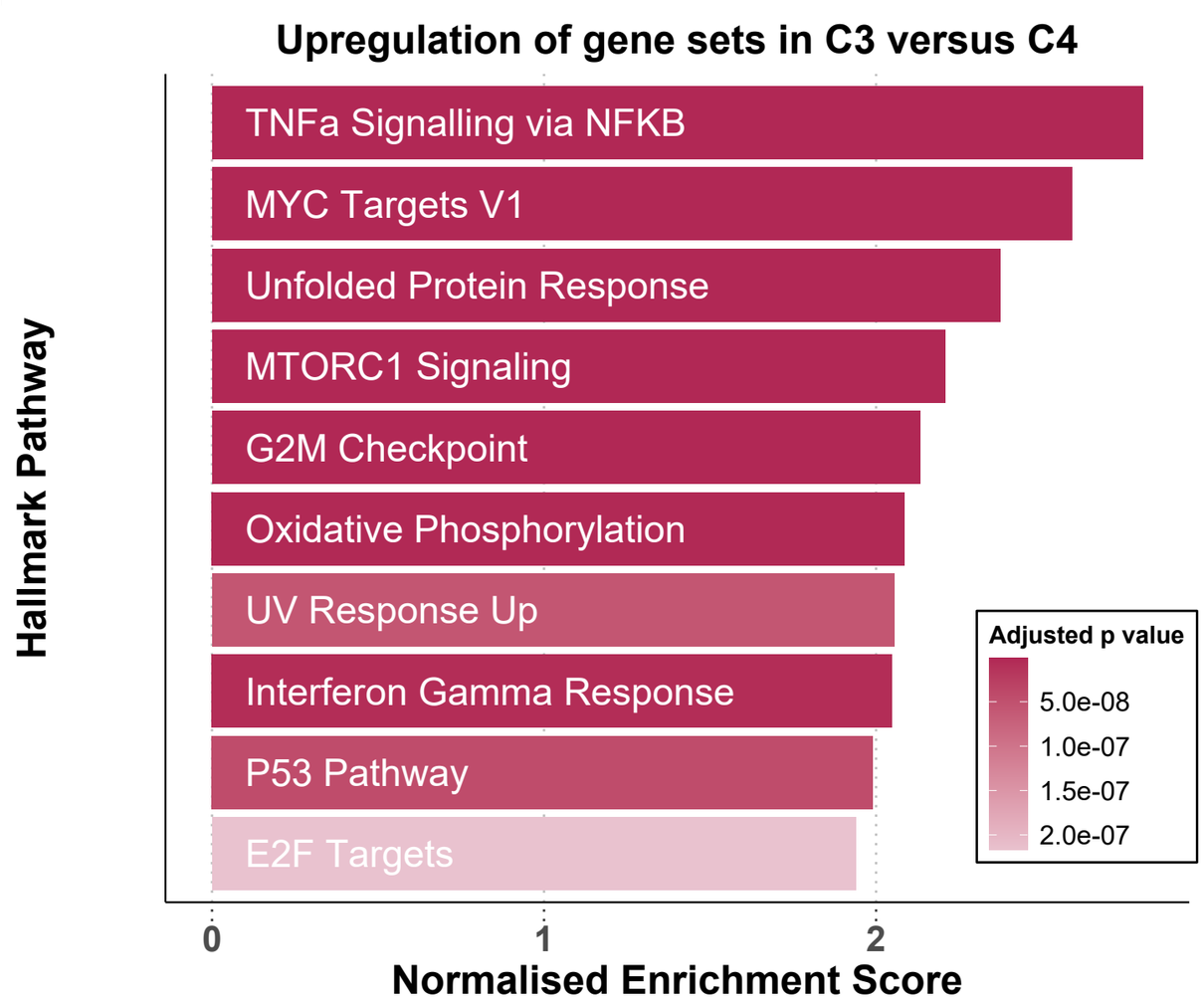

Figure 3

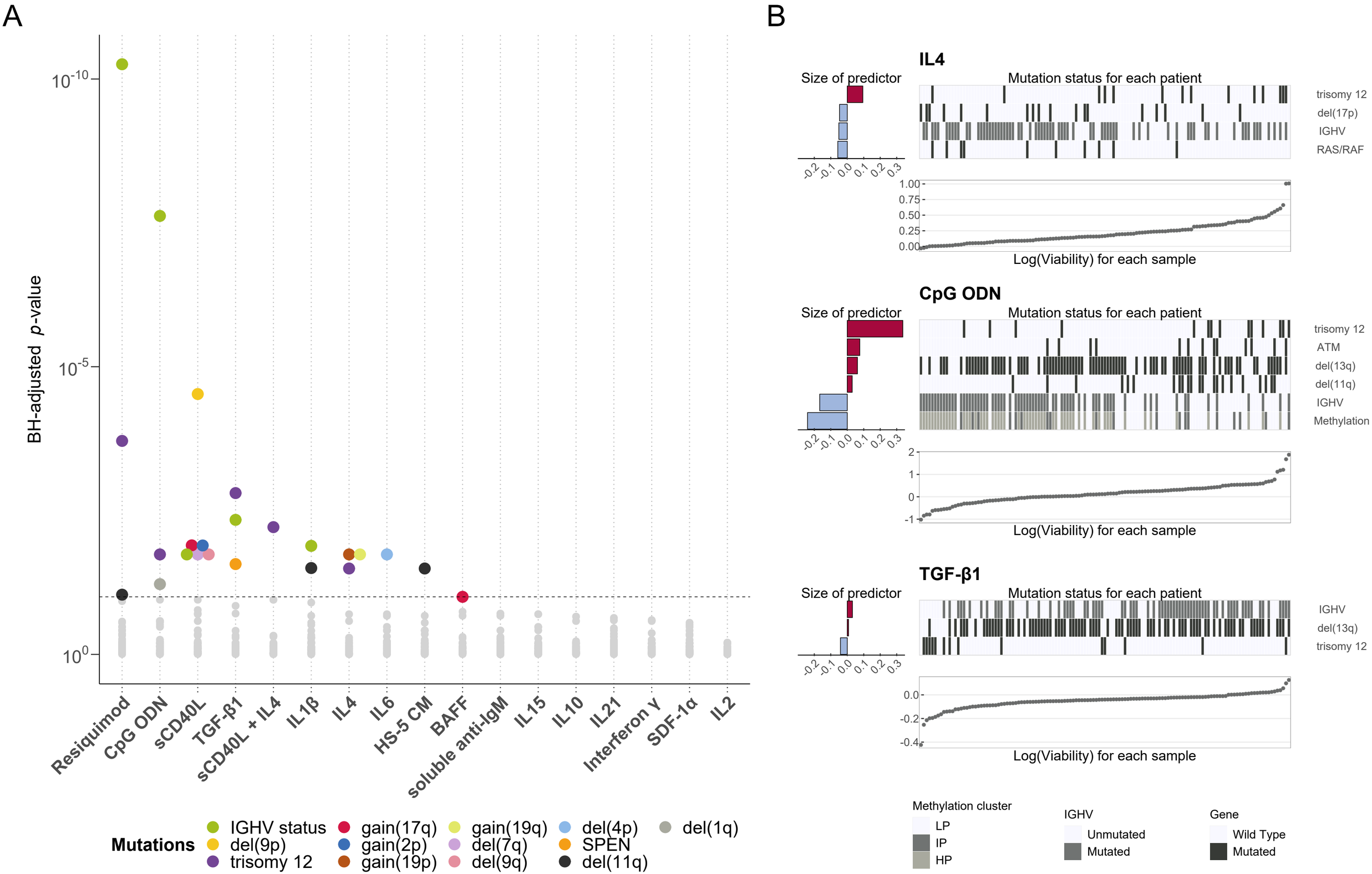
A
BH-adjusted p-value
10^-10
10^-5
10^0
Resiquimod
CpG ODN
sCD40L
TGF-β1
sCD40L + IL4
IL1β
IL4
IL6
HS-5 CM
BAFF
soluble anti-IgM
IL15
IL10
IL21
Interferon γ
SDF-1α
IL2
Mutations
IGHV status
del(9p)
trisomy 12
gain(17q)
gain(2p)
gain(19p)
gain(19q)
del(7q)
del(9q)
del(4p)
SPEN
del(11q)
del(1q)
B
IL4
Size of predictor
Mutation status for each patient
trisomy 12
del(17p)
IGHV
RAS/RAF
Log(Viability) for each sample
CpG ODN
Size of predictor
Mutation status for each patient
trisomy 12
ATM
del(13q)
del(11q)
IGHV
Methylation
Log(Viability) for each sample
TGF-β1
Size of predictor
Mutation status for each patient
IGHV
del(13q)
trisomy 12
Log(Viability) for each sample
Methylation cluster
LP
IP
HP
IGHV
Unmutated
Mutated
Gene
Wild Type
Mutated

Figure 4

A

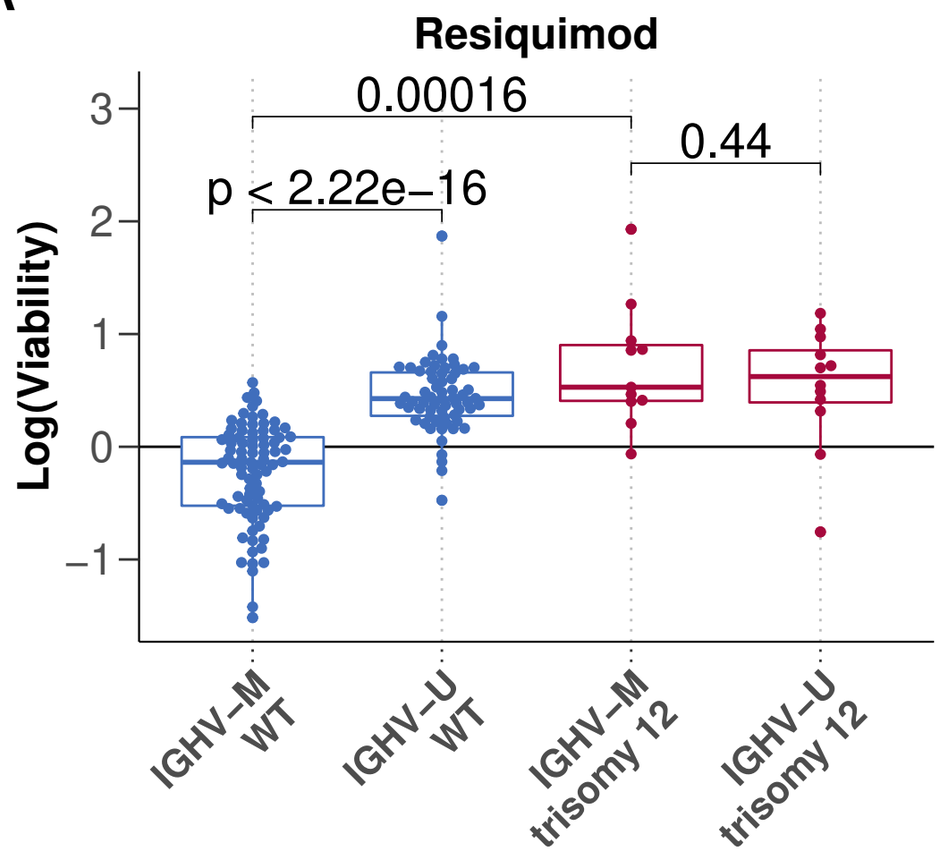

B

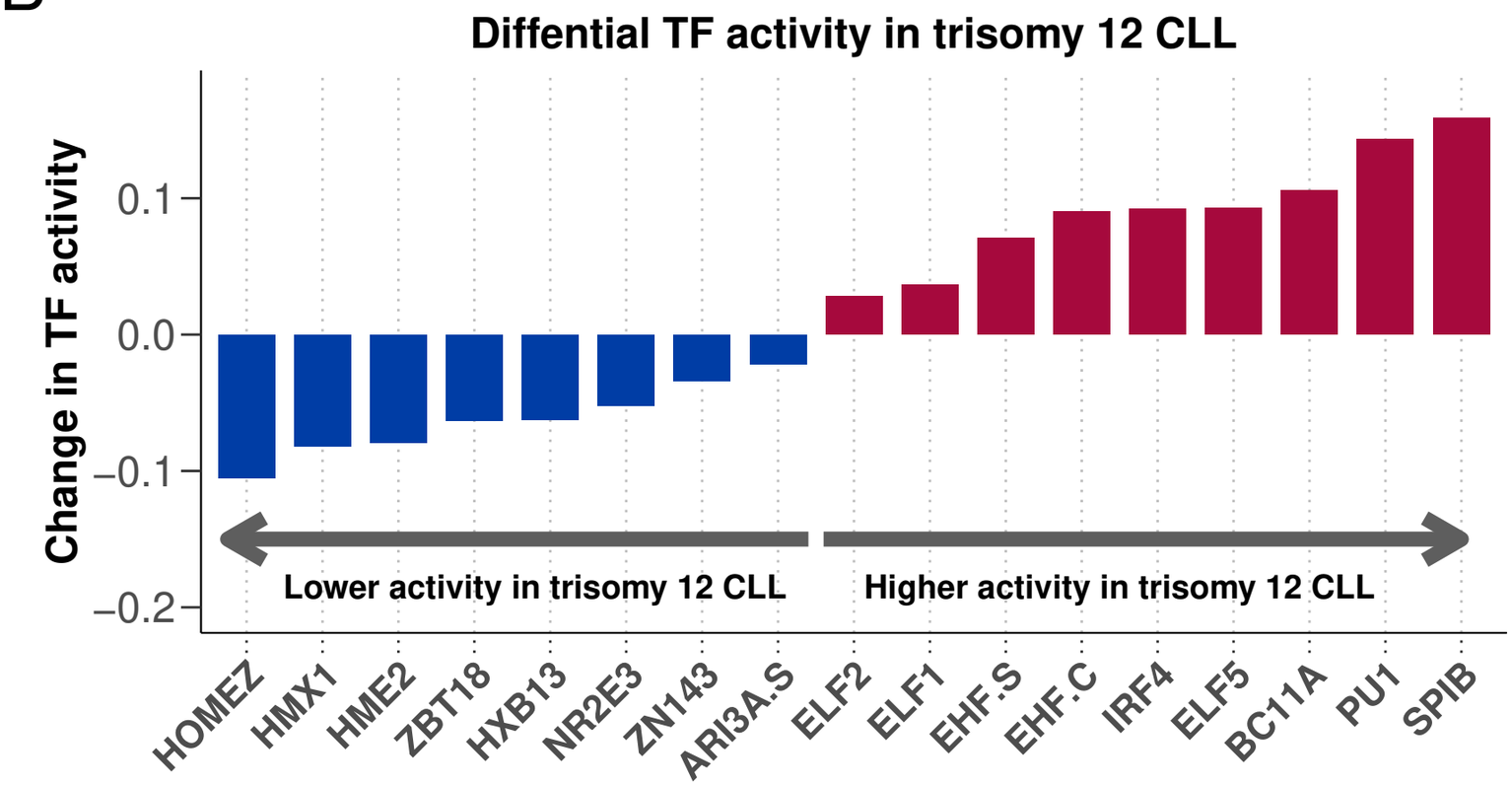

C

Pathway	Geneset Database	Geneset Size	Spi−B targets (/3253)	SPIB p−value	PU.1 targets (/250)	PU1 p−value
BCR Signaling Pathway	KEGG	75	36	0.000	4	0.056
TLR Signaling Pathway	KEGG	102	40	0.000	5	0.046
Signaling by TGFbeta Receptor Complex	Reactome	73	26	0.007	0	1.000

D

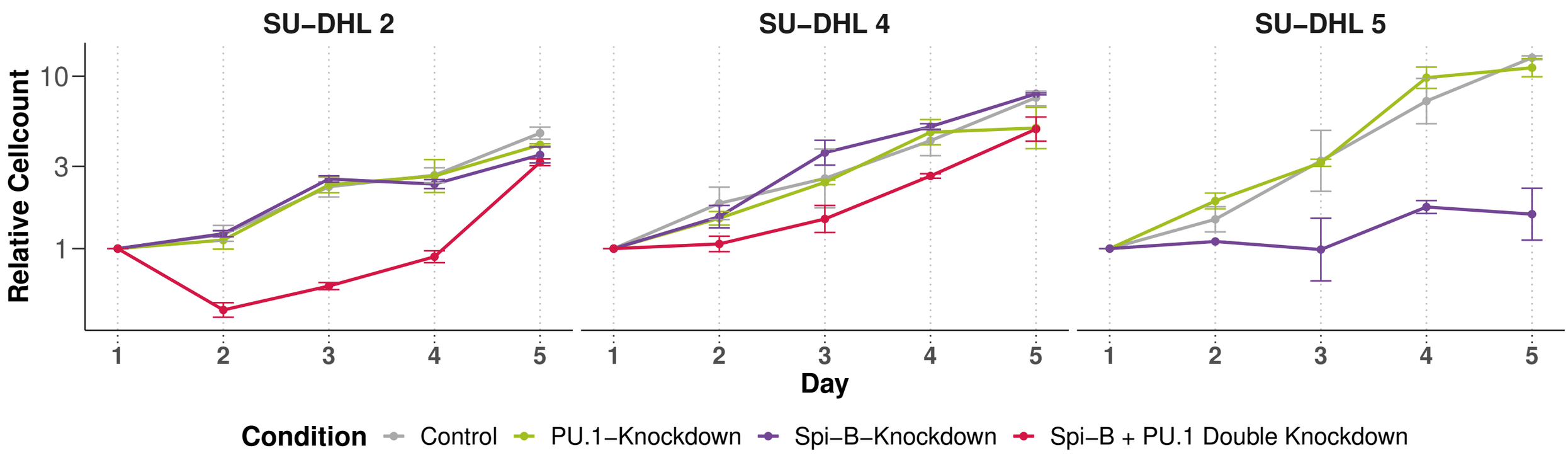

Figure 5

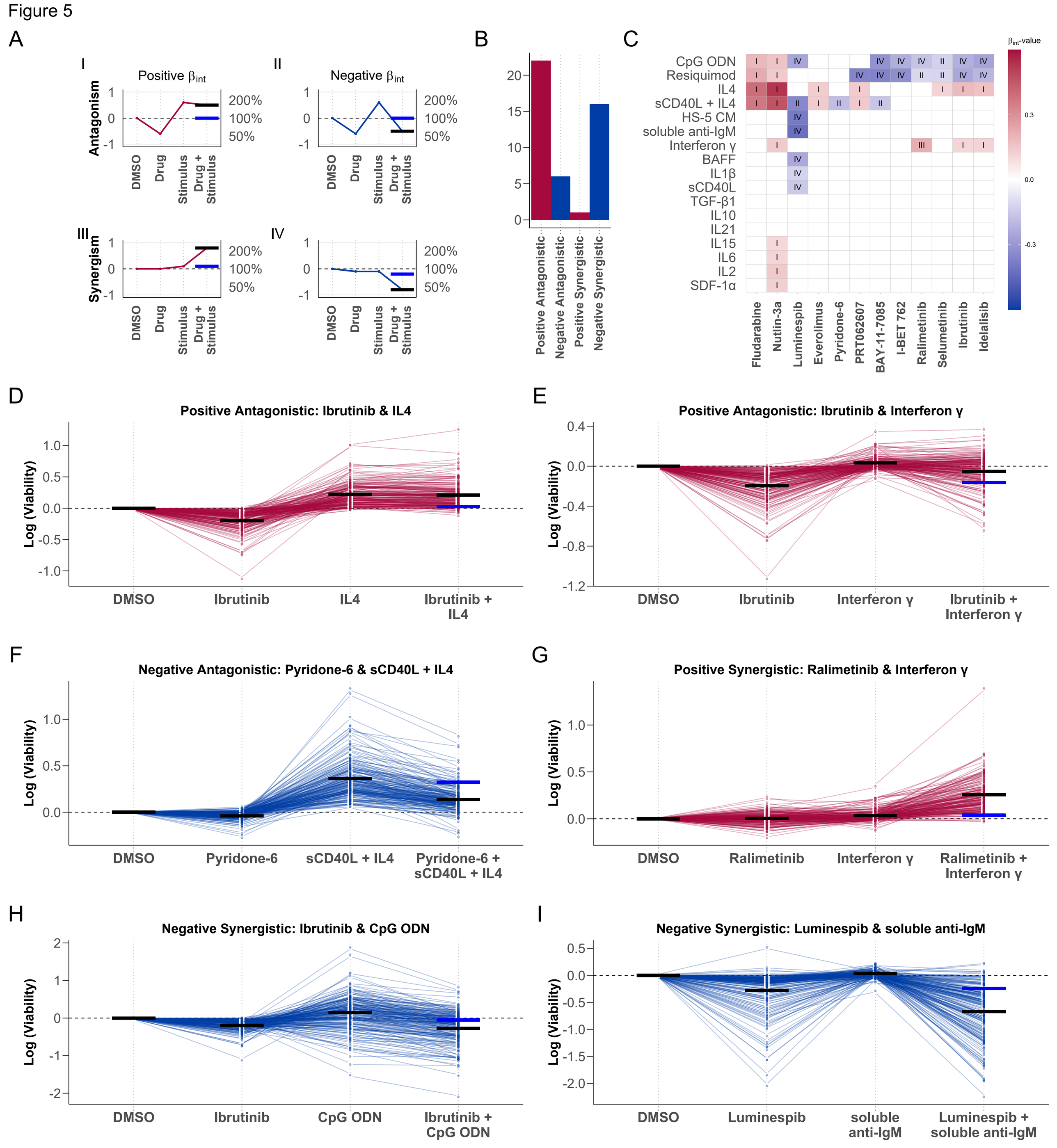
A
I
Positive β_{int}
Antagonism
II
Negative β_{int}
III
Synergism
IV
200%
100%
50%
DMSO
Drug
Stimulus
Drug + Stimulus
B
Positive Antagonistic
Negative Antagonistic
Positive Synergistic
Negative Synergistic
C
β_{int}-value
CpG ODN
Resiquimod
IL4
sCD40L + IL4
HS-5 CM
soluble anti-IgM
Interferon γ
BAFF
IL1β
sCD40L
TGF-β1
IL10
IL21
IL15
IL6
IL2
SDF-1α
Fludarabine
Nutlin-3a
Luminespib
Everolimus
Pyridone-6
PRT062607
BAY-11-7085
I-BET 762
Ralimetinib
Selumetinib
Ibrutinib
Idelalisib
D
Positive Antagonistic: Ibrutinib & IL4
Log (Viability)
DMSO
Ibrutinib
IL4
Ibrutinib + IL4
E
Positive Antagonistic: Ibrutinib & Interferon γ
Interferon γ
Ibrutinib + Interferon γ
F
Negative Antagonistic: Pyridone-6 & sCD40L + IL4
Pyridone-6
sCD40L + IL4
Pyridone-6 + sCD40L + IL4
G
Positive Synergistic: Ralimetinib & Interferon γ
Ralimetinib
Ralimetinib + Interferon γ
H
Negative Synergistic: Ibrutinib & CpG ODN
CpG ODN
Ibrutinib + CpG ODN
I
Negative Synergistic: Luminespib & soluble anti-IgM
Luminespib
soluble anti-IgM
Luminespib + soluble anti-IgM

Figure 6

A

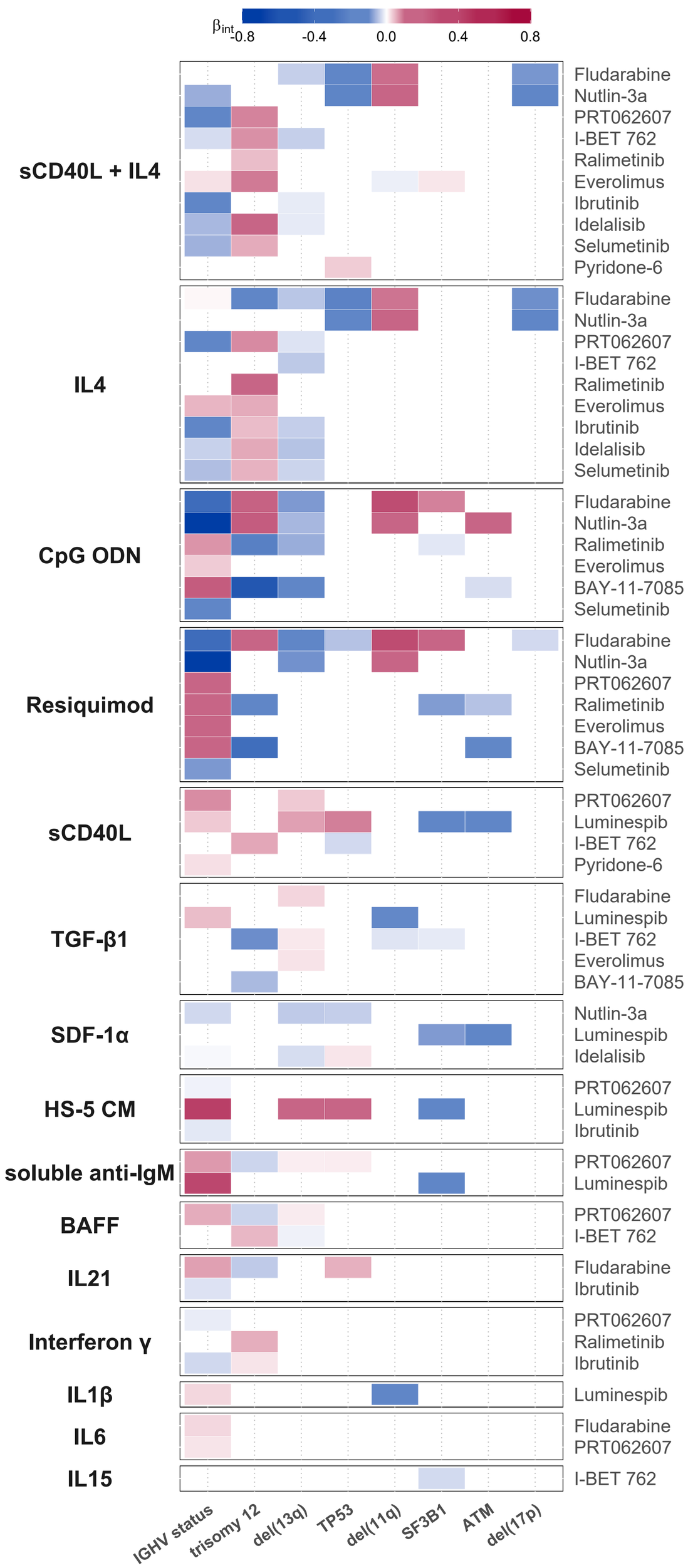

B

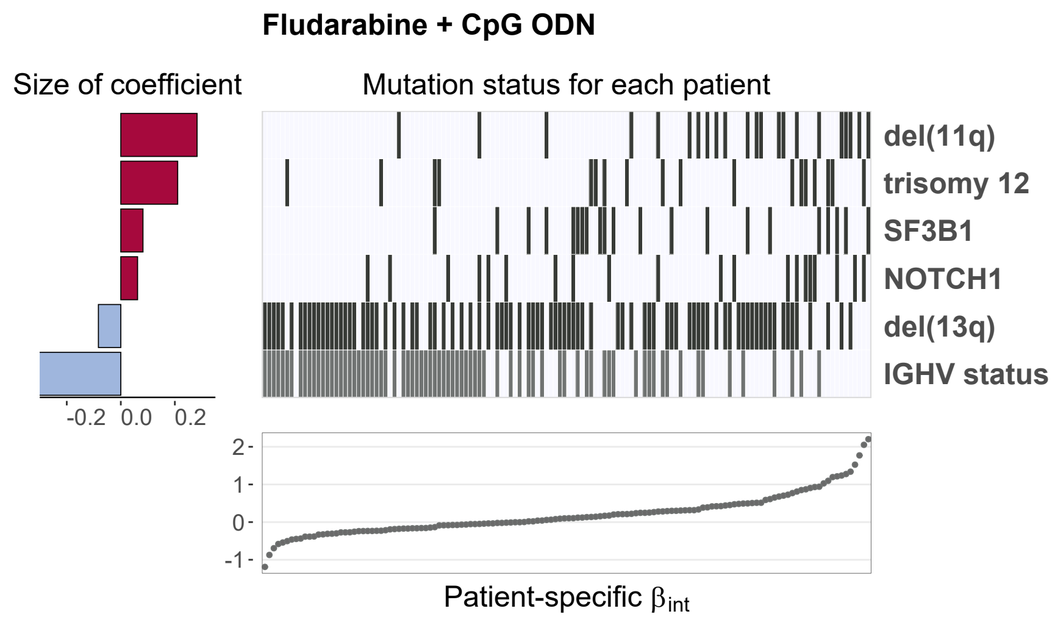

C

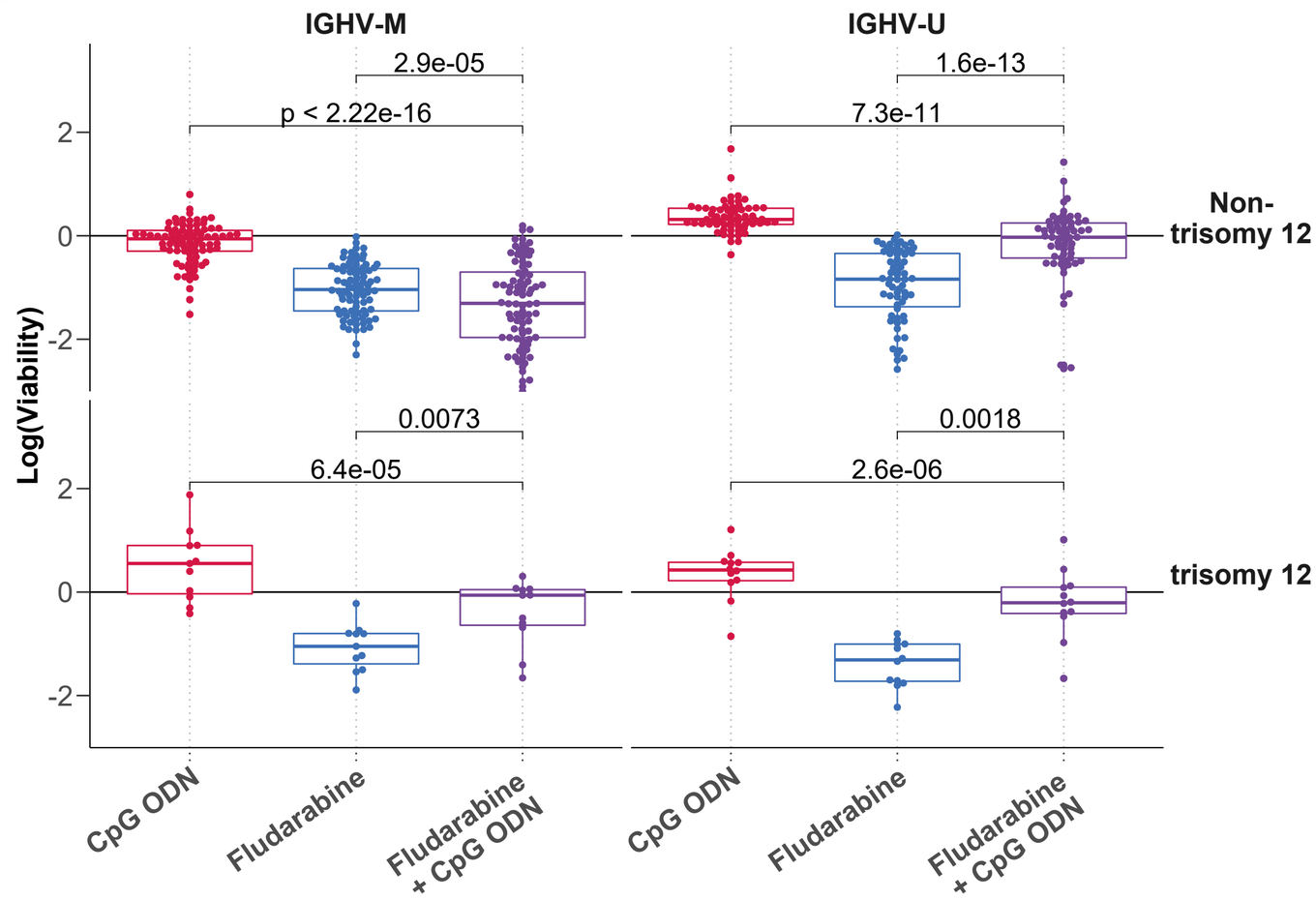

D

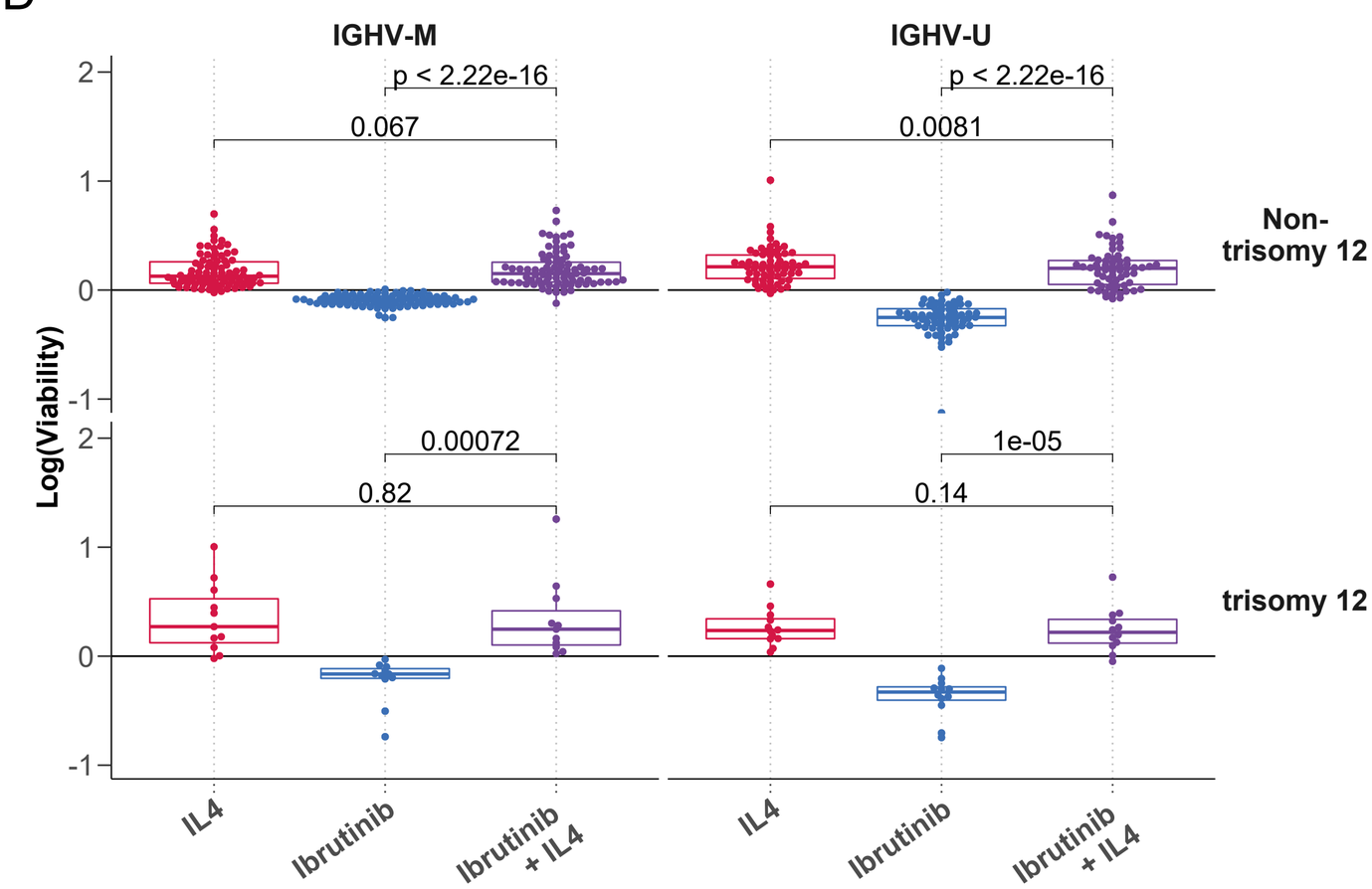

Figure 7

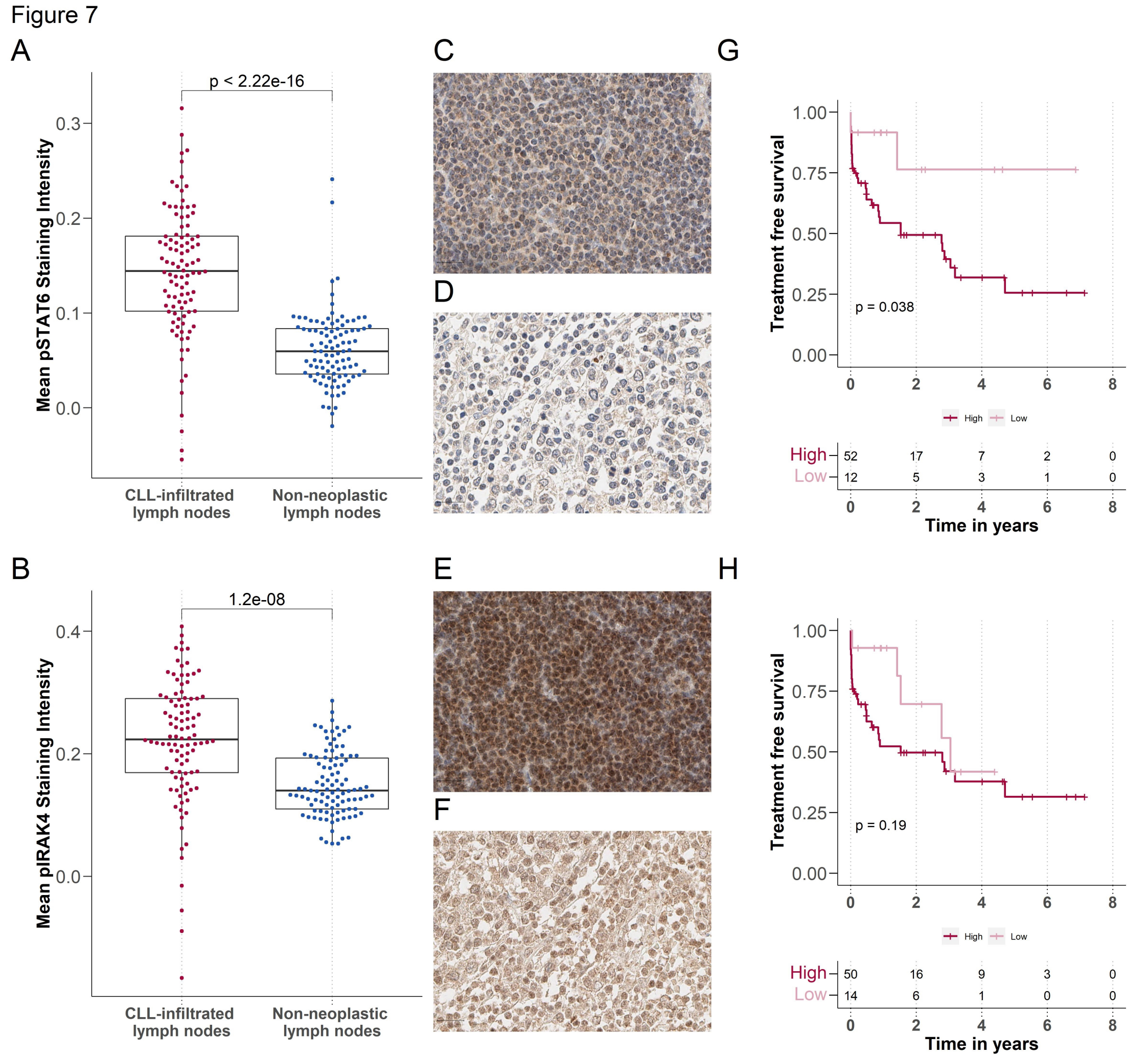
A
p < 2.22e-16
Mean pSTAT6 Staining Intensity
0.3
0.2
0.1
0.0
CLL-infiltrated lymph nodes
Non-neoplastic lymph nodes
C
D
G
Treatment free survival
1.00
0.75
0.50
0.25
0.00
p = 0.038
0
2
4
6
8
High
Low
High 52 17 7 2 0
Low 12 5 3 1 0
Time in years
B
1.2e-08
Mean pIRAK4 Staining Intensity
0.4
0.2
0.0
CLL-infiltrated lymph nodes
Non-neoplastic lymph nodes
E
F
H
Treatment free survival
1.00
0.75
0.50
0.25
0.00
p = 0.19
0
2
4
6
8
High
Low
High 50 16 9 3 0
Low 14 6 1 0 0
Time in years